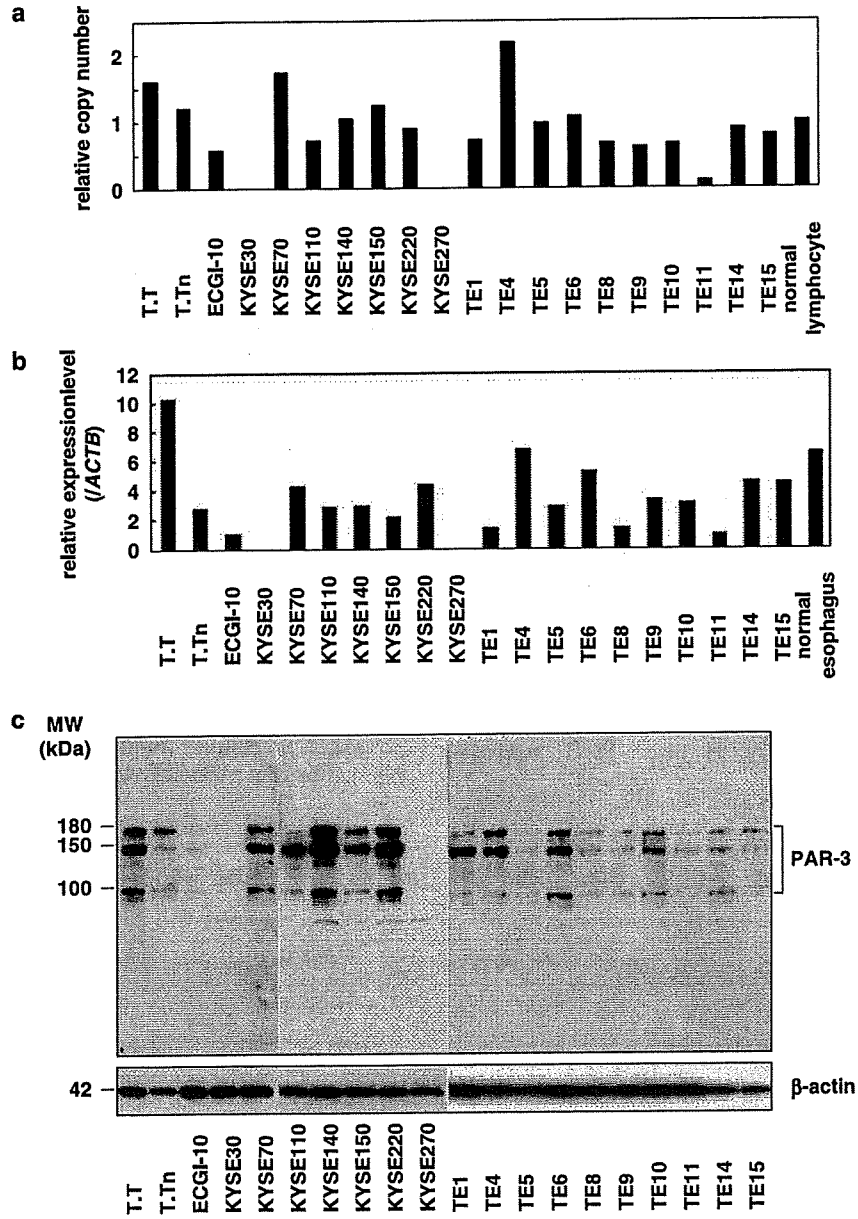

Figure 2 Copy number and expression level of *PARD3* in 20 ESCC cell lines. (**a**) The copy number of *PARD3* in 20 ESCC cell lines as measured by real-time quantitative PCR with reference to the LINE-1 control. Values are normalized such that the copy number in genomic DNA derived from normal lymphocytes has a value of 1. (**b**) Relative expression levels of *PARD3* in 20 ESCC cell lines and normal esophagus as evaluated by real-time quantitative reverse transcription (RT)–PCR. The results are presented as the expression level of each gene relative to a reference gene (*ACTB*) in order to correct for variations in the amount of RNA. (**c**) Immunoblot analyses of protein levels of PAR-3 in the indicated cell lines. β-Actin was used as an internal control.

of PAR-3 and ZO-1 by immunofluorescence in two *PARD3*-expressing cell lines (T.T and TE-4) with that in two cell lines lacking *PARD3* (KYSE30 and KYSE270). ZO-1 colocalized with PAR-3 at sites of cell–cell contact in T.T and TE-4 cells (Figure 3a). In contrast, ZO-1 was only weakly observed at sites of cell–cell contact in KYSE30 cells and was barely detected in KYSE270 cells (Figure 3a), despite the fact that the ZO-1 protein could be detected by immunoblotting in all cell lines (Figure 3b). As expected, the expression of PAR-3 was not detected in KYSE30 or KYSE270 cells (Figure 3a).

To further confirm that the absence of PAR-3 was the cause of the aberrant localization of ZO-1 in the KYSE30 and KYSE270 cells, we determined whether transfection of *PARD3* into these cells could restore ZO-1 localization to tight junctions. After transfection, the expression of PAR-3 (molecular weight, 180 kDa) in the *PARD3*-transfected KYSE30 and KYSE270 cells was detected by immunoblotting analysis (Figure 4a).

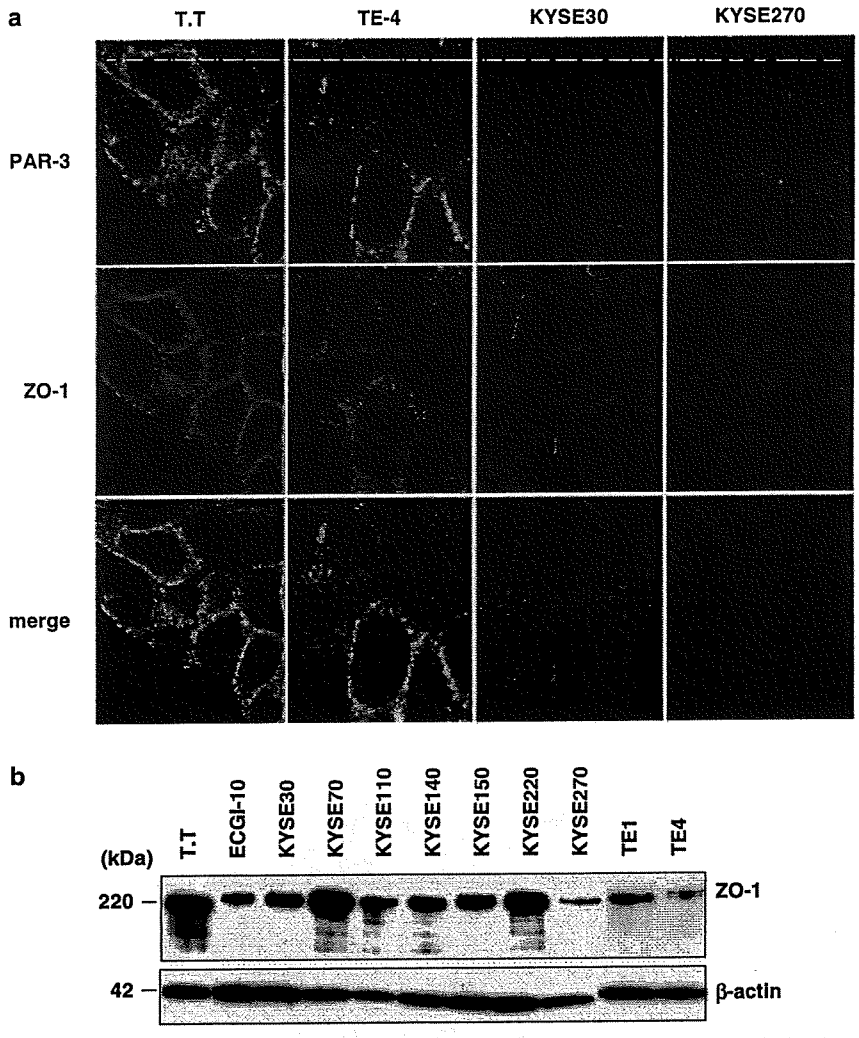

Figure 3 Effect of *PARD3* deletion on the subcellular localization of ZO-1. (**a**) Subcellular localization of PAR-3 and ZO-1 in PAR-3-expressing (T.T, TE-4) and non-expressing (KYSE30, KYSE270) cells. The cells were doubly stained with anti-PAR-3 (green) and anti-ZO-1 (red), and were viewed with a confocal laser scanning microscope. PAR-3 and ZO-1 colocalized at cell–cell borders in the T.T and TE-4 cells. The nuclear staining observed with anti-PAR-3 in the KYSE30 and KYSE270 cells is probably nonspecific because of the absence of *PARD3*. Original magnifications, × 1000. (**b**) Immunoblotting analyses of ZO-1 and β-actin, used as an internal control, in 11 ESCC cell lines.

Immunocytochemistry showed that, in addition to a diffuse staining, PAR-3 could now be detected in a linear manner at cell–cell borders in the *PARD3*-transfected KYSE30 and KYSE270 cells, in which it colocalized with ZO-1 (Figure 4b). Transfection of *PARD3* led to a stronger staining of ZO-1 at sites of cell–cell contact compared with control-transfected cells (Figure 4b). This was despite the fact that the total level of ZO-1 was the same in *PARD3* and control transfectants (Figure 4c). Knockdown of the *PARD3* expression in T.T cells was carried out using RNA interference (RNAi). After treatment of T.T cells with small interfering RNA (siRNA) targeting *PARD3*, we observed a decrease in the PAR-3 protein level relative to that observed for cells receiving negative control siRNA, transfection agent alone or left untreated (Figure 4a). Suppression of the PAR-3 expression by siRNA caused a disruption of localization of ZO-1 at cell–cell borders (Figure 4b), although the total level of ZO-1 was unchanged (Figure 4c). Taken together, these findings suggest that PAR-3 promotes the recruitment of ZO-1 to sites of cell–cell contact.

PAR-3 and cell migration

To investigate the role of PAR-3 in cell motility, we performed a monolayer wound-healing assay in knockdown T.T cells. Knockdown of the *PARD3* expression was conducted as described above. Wound closure was shown to be unchanged among *PARD3* siRNA-treated cells, negative control siRNA-treated cells and untreated cells (Supplementary Figure S2).

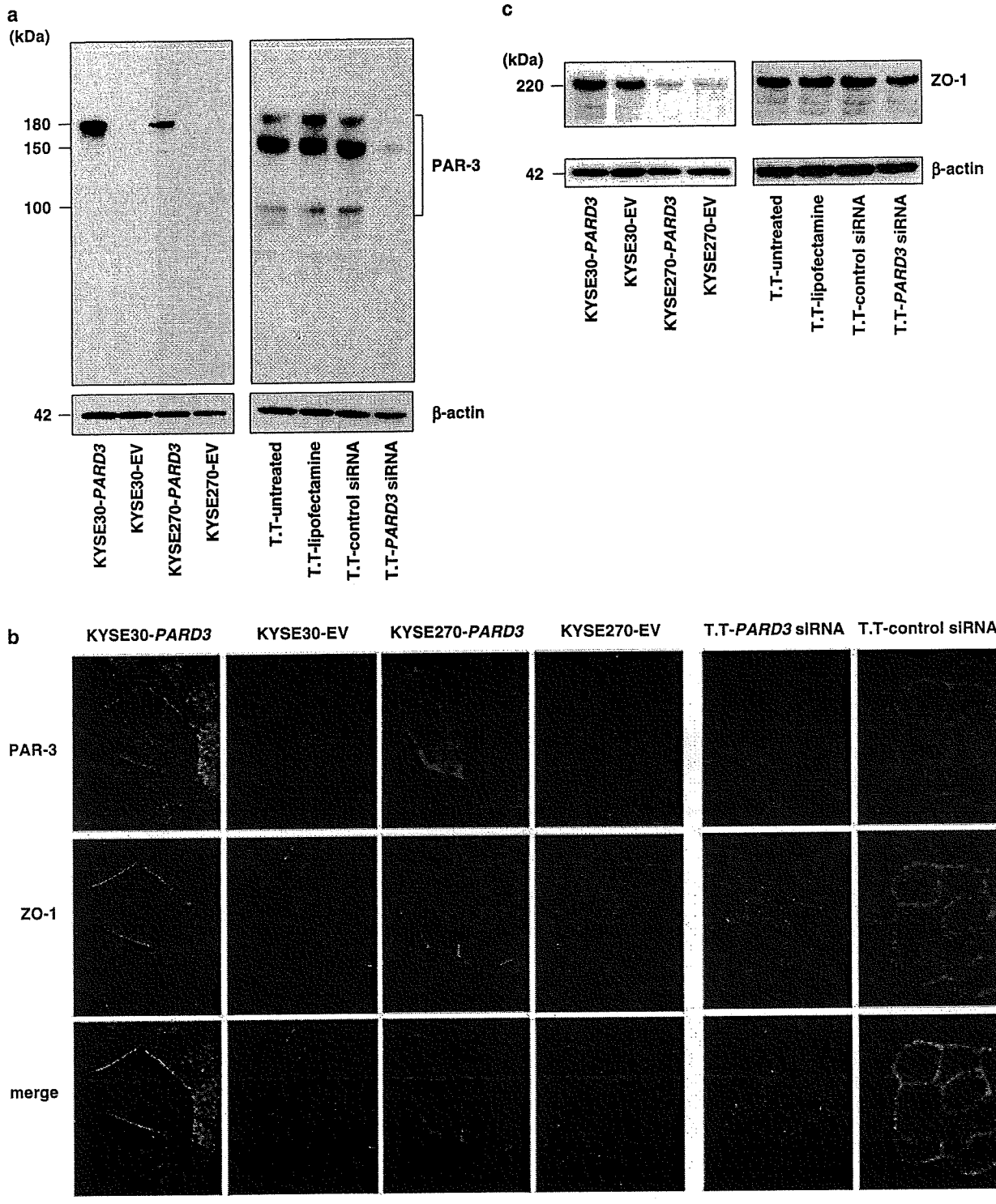

Figure 4 Effect of enforced expression of *PARD3* or knockdown of *PARD3* expression on the subcellular localization of ZO-1. KYSE30 and KYSE270 cells were transfected with the *PARD3* expression vector or with an empty vector (EV). T.T cells were treated with siRNA targeting *PARD3*, control siRNA, transfection agent (lipofectamine) alone or left untreated. (**a**) Immunoblot analysis of PAR-3. Analysis of β-actin served as an internal control. (**b**) Subcellular localization of PAR-3 and ZO-1 in transiently transfected cells. The cells were doubly stained with anti-PAR-3 (green) and anti-ZO-1 (red), and were viewed with a confocal laser scanning microscope. Original magnification, × 1000. (**c**) Immunoblot analyses of ZO-1 and an internal control, β-actin.

This suggests that the suppression of PAR-3 may not affect cell migration.

Analysis of PARD3 *defects in primary tumors*

To determine whether the loss of *PARD3* observed in KYSE30 and KYSE270 carcinoma cell lines was relevant to primary carcinomas in humans, we first determined the DNA copy number of *PARD3* in 40 primary ESCC tumors (Figure 5a). For this analysis, the values were normalized such that the copy number in genomic DNA derived from normal lymphocytes was given a value of 1. Copy number changes were counted as losses if the results of the analysis for a given ESCC tumor were <0.7 (Berggren *et al.*, 2003). Using these parameters, a copy number loss of *PARD3* was observed in 6 (15%) of the 40 tumors.

We then further quantified the mRNA levels of *PARD3* in the available paired tumor and nontumor tissues from 33 ESCC patients (Figure 5b). Patient and tumor characteristics are summarized in Supplementary Table S2. The expression of *PARD3* mRNA was significantly reduced in 23 (70%) of the 33 tumors when compared with their nontumorous tissue counterparts (Wilcoxon signed-rank test, $P=0.017$). To clarify the relationship between the expression level of *PARD3* and various clinicopathological parameters, we correlated the *PARD3* expression level with clinical data that was available for 28 of the patients. For this purpose, tumors were divided into one of two groups based on reduction in *PARD3* levels: tumor tissue (T) <nontumor tissue (NT), or not reduced (T≥NT). Reduced expression of *PARD3* was significantly associated with a younger age (≤65 years), positive lymph node metastasis and poor differentiation (Table 1). These findings suggest that reduced expression of *PARD3* is important not only for cancer cell lines but also for the tumorigenic properties of primary tumors.

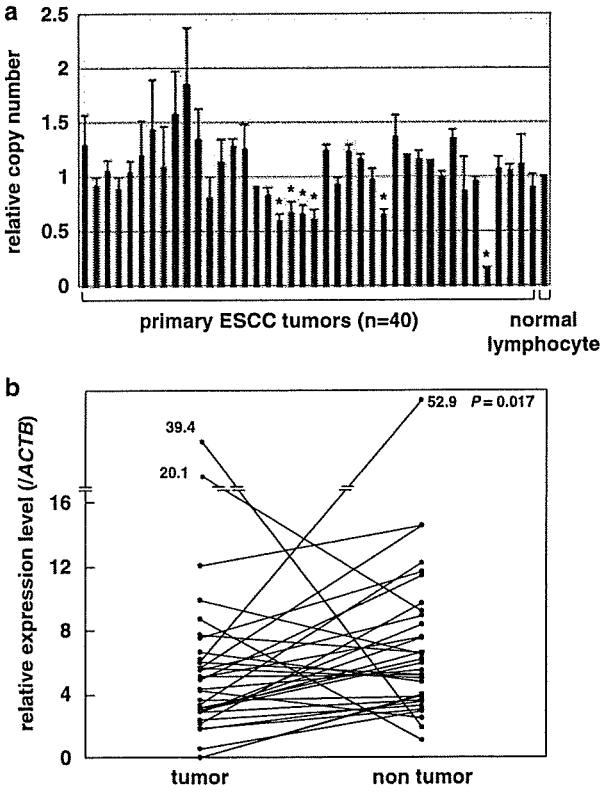

Figure 5 Copy number and expression level of *PARD3* in primary ESCC tumors. (a) The copy number of *PARD3* in each of 40 primary ESCC tumors was determined as described in Figure 2a. Values are represented as the mean ± s.d. of three independent experiments. Asterisks indicate tumors with a loss (<0.7) of *PARD3*. The copy number of normal lymphocytes served as a control. (b) The relative expression of *PARD3* in paired tumor (T) and nontumor tissues (NT) from 33 patients with primary ESCCs was determined as described in Figure 2b. *P*-values of <0.05 were considered significant.

Discussion

Homozygous deletions have been useful in the positional cloning of a number of tumor suppressor

Table 1 Relationship between clinicopathological features and levels of expression of *PARD3* in 28 primary ESCCs

Characteristics	*PARD3*		P-*value*[a]
	T<NT (n=*18*)	*T≥NT* (n=*10*)	
Age (years)			
≤65	11	2	0.037
>65	7	8	
Gender			
Male	14	8	0.891
Female	4	2	
Tumor diameter (cm)			
≤3 cm	6	7	0.062
>3 cm	12	3	
Stage			
I/II	8	7	0.194
III/IV	10	3	
T classification			
T1/T2	8	7	0.194
T3/T4	10	3	
N status			
N0	5	7	0.031
N1	13	3	
M status			
M0	15	10	0.172
M1	3	0	
Histological differentiation			
Well/moderate	11	10	0.023
Poor	7	0	

Abbreviations: ESCC, esophageal squamous cell carcinoma; NT, nontumor tissue; T, tumor tissue.
[a]χ^2-Test.

genes (Friend *et al.*, 1986; Kamb *et al.*, 1994; Hahn *et al.*, 1996; Li *et al.*, 1997). A putative tumor suppressor is believed to lie on the chromosomal region 10p in ESCC (Aoki *et al.*, 1994). In this study, using high-density SNP arrays, we identified a novel homozygous deletion at the chromosomal region 10p11 in 2 out of 20 ESCC cell lines. Subsequent detailed analyses narrowed down the extent of the shortest region of overlap of the homozygous deletions to exons 3–22 of the gene *PARD3*. Recently, homozygous deletion of *PARD3* has been reported in two lung cancer cell lines (Nagayama *et al.*, 2007).

A few studies have suggested an association of *PARD3* with tumors (Fang and Xu, 2001; Zitzelsberger *et al.*, 2004), and *PARD3* was reported to be amplified in radiation-transformed neoplastic retinal pigment epithelial cell lines (Zitzelsberger *et al.*, 2004). Also, various splicing transcripts of *PARD3* are expressed in primary hepatocellular carcinomas, and the expression of exon 17b deleted *PARD3* variants is downregulated in these carcinomas compared with the surrounding nontumorous liver tissues (Fang and Xu, 2001). However, the biological function of *PARD3* and its clinical significance for cancer are poorly understood. In this study, a gain of *PARD3* copy number (defined as twice the level of normal DNA) was observed in only 1 of the 20 ESCC cell lines tested (TE4 cells) and in none of the 40 primary ESCC tumors analysed. Conversely, a loss of *PARD3* was detected in 15% of the primary ESCC tumors examined, and a reduced expression of *PARD3* mRNA was found in primary ESCC tumors compared with their nontumorous counterparts. The reduced expression of *PARD3* was associated with aggressive ESCC phenotypes, such as positive lymph node metastasis and poor differentiation. To validate these results at the protein level, we unsuccessfully tried to carry out the immunohistochemical analysis of PAR-3 on formalin-fixed and paraffin-embedded sections of primary ESCC specimens. We assume that the anti-PAR-3 antibody is not suitable for formalin-fixed and paraffin-embedded sections. Further studies in more numerous primary samples and studies using immunohistochemistry are needed to determine the clinical importance of PAR-3 in ESCC.

PAR-3 has been implicated in the formation of normal tight junctions at epithelial cell–cell contacts (Joberty *et al.*, 2000; Macara, 2004; Chen and Macara, 2005; Suzuki and Ohno, 2006). PAR-3 plays the role of a scaffold in the recruitment of proteins, such as PAR-6 or aPKC, that are involved in the formation of these junctions (Assémat *et al*, 2008). In agreement with these data, our immunocytochemical analyses showed that PAR-3 colocalized with the tight junction component, ZO-1, at sites of cell–cell contact in T.T and TE-4 cells that express *PARD3*. Unexpectedly, ZO-1 was weakly detected at sites of cell–cell contact in KYSE30 cells that lack *PARD3*. On the other hand, ZO-1 was barely detected in KYSE270 cells, which also lack *PARD3*. Exogenous expression of *PARD3* resulted in the recruitment of ZO-1 to sites of cell–cell contact in KYSE30 and KYSE270 cells without affecting the expression level of ZO-1. Conversely, knockdown of *PARD3* in T.T cells that express this gene caused a disruption of localization of ZO-1 at cell-cell borders. Taken together, these findings suggest that PAR-3 promotes the recruitment of ZO-1 to sites of cell–cell contact, although it may not always be essential for this localization of ZO-1. The finding that *PARD3* affects the formation of tight junction in ESCC cells might partially explain the observed association between the reduced expression of *PARD3* and positive lymph node metastasis, and between poor differentiation of primary ESCCs. However, our wound-healing assay did not show any effect of PAR-3 on cell migration. Further functional studies are needed to determine the implication of PAR-3 in ESCC invasion and metastasis.

Our finding that PAR-3 is important, but not essential, for tight junction formation and ZO-1 recruitment are in partial agreement with previous observations. The targeted disruption of the mouse PAR-3 gene (*Pard3*) results in embryonic lethality with defective epicardial development (Hirose *et al.*, 2006). *Pard3*-deficient epicardial progenitor cells do not form epicardial cysts from which the epicardium is derived. These cells show defects in the localization of PAR-6 and aPKC to the apical domain, but a normal localization of ZO-1 to cell–cell junctions. Interestingly, not all epithelial cells are affected in the *Pard3*-deficient embryo, which may be due to the proposed functional redundancy of PAR-3 and the PAR-3-related protein PAR-3L/PAR-3β (Gao *et al.*, 2002; Kohjima *et al.*, 2002). The function of PAR-3 has also been examined in MDCK II canine epithelial cells (Chen and Macara, 2005). In that study, withdrawal of calcium from the medium caused rapid loss of cell–cell junctions, which could be reversed by the re-addition of calcium (a calcium switch experiment). The normal relocalization of tight junction components at cell–cell contacts within 30 min after re-addition of calcium was profoundly delayed in cells lacking PAR-3, although tight junctions could eventually form even without re-expression of PAR-3.

The exact mechanism by which PAR-3 modulates tight junctions and contributes to tumorigenicity remains to be elucidated. Besides PAR-6 and aPKC, PAR-3 also interacts with other proteins such as 14-3-3, LIMK2 and the Rac-specific guanine nucleotide exchange factor STEF/Tiam1 (Humbert *et al.*, 2006; Assémat *et al.*, 2008). Moreover, recent studies have shown that the PAR-3–PAR-6–aPKC complex associates with the tumor suppressor VHL (von Hippel–Lindau protein) or with PTEN (phosphatase and tensin homologue deleted on chromosome ten) (Wodarz and Näthke, 2007), suggesting potential mechanisms by which PAR-3 might modulate tumorigenicity. Although the mechanism of PAR-3 function in tumors remains to be elucidated and the findings must be verified in a larger sample number, the data presented in this work clearly suggest a role for PAR-3 deletion in the tumorigenesis of ESCC.

Materials and methods

Cell lines and primary tumors

The ESCC cell lines TE-1, TE-5, TE-9, TE-15 and EC-GI-10 were obtained from RIKEN Bioresource Center (Tsukuba, Japan); T.T, T.Tn, KYSE30, KYSE70, KYSE110, KYSE140, KYSE150, KYSE220 and KYSE270 were from Japan Health Sciences Foundation (Osaka, Japan); and TE-4, TE-6, TE-8, TE-10, TE-11 and TE-14 were from Cell Resource Center for Biomedical Research, Tohoku University (Sendai, Japan). All cell lines were maintained in Dulbecco's modified Eagle's medium supplemented with 10% fetal bovine serum. Genomic DNA was isolated from the cell lines with the DNeasy Mini Kit (Qiagen, Tokyo, Japan).

Paired tumor and nontumor tissues were obtained during upper gastrointestinal endoscopic inspection from 40 ESCC patients who underwent biopsy for diagnostic purposes at the Hospital of Kyoto Prefectural University of Medicine (Kyoto, Japan). All biopsy specimens were immediately frozen in liquid nitrogen and stored at −80 °C until required. Genomic DNA and total RNA were isolated from primary samples with the AllPrep DNA/RNA Mini Kit (Qiagen). All tumor samples were available for DNA analyses, and 33 paired tumor and nontumor samples were available for mRNA analyses. Before the study, informed consent was obtained and the study was approved by ethics committees.

Array analysis

Array analyses were carried out with the GeneChip Mapping 250K Sty array (Affymetrix, Santa Clara, CA, USA) according to the manufacturer's instructions. In brief, 250 ng of genomic DNA was digested with a restriction enzyme (*StyI*), ligated to an adaptor and amplified by PCR. Amplified products were fragmented, labeled by biotinylation and hybridized to the microarrays. Hybridization was detected by incubation with streptavidin–phycoerythrin conjugates, followed by scanning of the array, and analysis was carried out as described earlier (Kennedy *et al.*, 2003). Copy number changes were calculated using the Copy Number Analyzer for Affymetrix GeneChip Mapping Arrays (CNAG; http://www.genome.umin.jp; Nannya *et al.*, 2005).

PCR analysis

Conventional PCR was performed using Ex Taq DNA Polymerase (Takara, Otsu, Japan) as described by the manufacturer. Genomic DNA and mRNA were quantified with a real-time fluorescence detection method as described earlier (Inagaki *et al.*, 2008). Total RNA derived from normal human esophageal epithelial cells was purchased from Ambion (Austin, TX, USA). Single-stranded cDNAs were generated from total RNAs using QuantiTect Reverse Transcription Kit (Qiagen). Primers used for genomic PCR and RT–PCR are listed in Supplementary Table S1. Endogenous controls for mRNA and genomic DNA levels were *ACTB* and the long interspersed nuclear element 1 (LINE-1) (Zhao *et al.*, 2004), respectively.

Immunoblotting

Immunoblots were prepared according to the previously reported methods (Yasui *et al.*, 2001). Cell lysates (20 μg protein per sample) were separated by SDS–polyacrylamide gel electrophoresis using 10% acrylamide gels. The anti-PAR-3 polyclonal antibody was obtained from Upstate Biotechnology (Lake Placid, NY, USA), the anti-β-actin monoclonal antibody from Sigma-Aldrich (Tokyo, Japan) and the anti-ZO-1 monoclonal antibody from Zymed (South San Francisco, CA, USA). The anti-PAR-3, anti-ZO-1 and anti-β-actin antibodies were used for immunoblotting at dilutions of 1:500, 1:250 and 1:5000, respectively. For secondary immunodetection, anti-rabbit or anti-mouse immunoglobulin (Ig) (Amersham, Tokyo, Japan) was diluted 1:5000. Protein binding was detected using the ECL system (Amersham).

Transient expression of PARD3

The full-length human *PARD3* cDNA (clone ID: IOH62499) was obtained from Invitrogen (Carlsbad, CA, USA) and was subcloned into pcDNA3.2/V5-DEST vector (Invitrogen) to generate a mammalian expression vector. The *PARD3* expression vector, or an empty vector, was transfected into KYSE30 and KYSE270 cells using the Effectene Transfection Reagent Kit (Qiagen) according to the manufacturer's instructions. After 48 h incubation, the cell lysates were analysed by immunoblotting for detection of the expression of PAR-3 protein.

RNAi

Small interfering RNA duplex oligoribonucleotides targeting *PARD3* (5′-AAUGAUGGGUGUACGCAUGGCUUGG-3′) and control (non-silencing) siRNA duplexes were synthesized by Invitrogen in order to investigate the role of PAR-3 in ZO-1 localization and cell motility. The siRNAs were delivered into T.T cells using Lipofectamine RNAiMAX (Invitrogen), according to the manufacturer's protocol.

Immunofluorescence microscopy

KYSE30 and KYSE270 cells were transfected with the *PARD3* expression vector or the empty vector. T.T cells were transfected with either siRNA targeting *PARD3* or negative control siRNA. After 24 h incubation, the cells were collected, reseeded on glass slides and incubated overnight. The cells were fixed with 3.7% formaldehyde, permeabilized with 0.2% Triton X-100 and incubated with phosphate-buffered saline containing 1% bovine serum albumin. The cells were then treated with a mixture of anti-PAR-3 and anti-ZO-1 antibodies at a dilution of 1:500 and 1:100, respectively, for 1 h at 37 °C. The second antibodies used were a mixture of fluorescein isothiocyanate-conjugated anti-rabbit Ig (Cappel, Aurora, OH, USA) and rhodamine-conjugated anti-mouse Ig (Cappel) for the detection of PAR-3 and ZO-1, respectively. Samples were examined using a confocal laser scanning microscope (SV1000; Olympus, Tokyo, Japan).

Monolayer wound healing assay

T.T cells were transfected with either siRNA targeting *PARD3* or negative control siRNA, or left untreated. After 24 h, cells in Dulbecco's modified Eagle's medium with 1% fetal bovine serum were seeded on glass slides and allowed to adhere overnight. Wounds were scratched into the cell monolayer using a sterile 200-μl pipette tip, rinsed the cells with phosphate-buffered saline and added Dulbecco's modified Eagle's medium containing 10% fetal bovine serum with mitomycin C (0.5 μg/ml, Nacalai Tesque, Kyoto, Japan). Mitomycin C blocks mitosis and thus allows analysis of cell migration in the absence of cell proliferation. Cells were allowed to migrate into the wound over a period of 24 h before fixation. Wound widths were measured in three randomly selected regions at 0, 12 and 24 h after wounding. Cells were stained with Giemsa stain (Nacalai Tesque, Kyoto, Japan). Experiments were repeated at least three times.

Statistical analysis
Statistical analyses were carried out using SPSS 15.0 software (SPSS, Chicago, IL, USA). χ^2 or Wilcoxon signed-rank test was used. *P*-values of <0.05 were considered significant.

Conflict of interest

The authors declare no conflict of interest.

Acknowledgements

This study was supported by Grants-in-Aid for Scientific Research (18390223 and 20590408) from the Japan Society for the Program of Science (KY).

References

Aoki T, Mori T, Du X, Nisihira T, Matsubara T, Nakamura Y. (1994). Allelotype study of esophageal carcinoma. *Genes Chromosomes Cancer* **10**: 177–182.

Assémat E, Bazellières E, Pallesi-Pocachard E, Le Bivic A, Massey-Harroche D. (2008). Polarity complex proteins. *Biochim Biophys Acta* **1778**: 614–630.

Berggren P, Kumar R, Sakano S, Hemminki L, Wada T, Steineck G *et al.* (2003). Detecting homozygous deletions in the CDKN2A (p16(INK4a))/ARF(p14(ARF)) gene in urinary bladder cancer using real-time quantitative PCR. *Clin Cancer Res* **9**: 235–242.

Chen X, Macara IG. (2005). Par-3 controls tight junction assembly through the Rac exchange factor Tiam1. *Nat Cell Biol* **7**: 262–269.

Enzinger PC, Mayer RJ. (2003). Esophageal cancer. *N Engl J Med* **349**: 2241–2252.

Fang CM, Xu YH. (2001). Down-regulated expression of atypical PKC-binding domain deleted asip isoforms in human hepatocellular carcinomas. *Cell Res* **11**: 223–229.

Friend SH, Bernards R, Rogelj S, Weinberg RA, Rapaport JM, Albert DM *et al.* (1986). A human DNA segment with properties of the gene that predisposes to retinoblastoma and osteosarcoma. *Nature* **323**: 643–646.

Gao L, Macara IG, Joberty G. (2002). Multiple splice variants of Par3 and of a novel related gene, Par3L, produce proteins with different binding properties. *Gene* **294**: 99–107.

Hahn SA, Schutte M, Hoque AT, Moskaluk CA, da Costa LT, Rozenblum E *et al.* (1996). DPC4, a candidate tumor suppressor gene at human chromosome 18q21.1. *Science* **271**: 350–353.

Hirose T, Karasawa M, Sugitani Y, Fujisawa M, Akimoto K, Ohno S *et al.* (2006). PAR3 is essential for cyst-mediated epicardial development by establishing apical cortical domains. *Development* **133**: 1389–1398.

Humbert PO, Dow LE, Russell SM. (2006). The Scribble and Par complexes in polarity and migration: friends or foes? *Trends Cell Biol* **16**: 622–630.

Inagaki Y, Yasui K, Endo M, Nakajima T, Zen K, Tsuji K *et al.* (2008). CREB3L4, INTS3, and SNAPAP are targets for the 1q21 amplicon frequently detected in hepatocellular carcinoma. *Cancer Genet Cytogenet* **180**: 30–36.

Izumi Y, Hirose T, Tamai Y, Hirai S, Nagashima Y, Fujimoto T *et al.* (1998). An atypical PKC directly associates and colocalizes at the epithelial tight junction with ASIP, a mammalian homologue of *Caenorhabditis elegans* polarity protein PAR-3. *J Cell Biol* **143**: 95–106.

Joberty G, Petersen C, Gao L, Macara IG. (2000). The cell-polarity protein Par6 links Par3 and atypical protein kinase C to Cdc42. *Nat Cell Biol* **2**: 531–539.

Kamb A, Gruis NA, Weaver-Feldhaus J, Liu Q, Harshman K, Tavtigian SV *et al.* (1994). A cell cycle regulator potentially involved in genesis of many tumor types. *Science* **264**: 436–440.

Kemphues KJ, Priess JR, Morton DG, Cheng NS. (1988). Identification of genes required for cytoplasmic localization in early *C. elegans* embryos. *Cell* **52**: 311–320.

Kennedy GC, Matsuzaki H, Dong S, Liu WM, Huang J, Liu G *et al.* (2003). Large-scale genotyping of complex DNA. *Nat Biotechnol* **21**: 1233–1237.

Kohjima M, Noda Y, Takeya R, Saito N, Takeuchi K, Sumimoto H. (2002). PAR3beta, a novel homologue of the cell polarity protein PAR3, localizes to tight junctions. *Biochem Biophys Res Commun* **299**: 641–646.

Li J, Yen C, Liaw D, Podsypanina K, Bose S, Wang SI *et al.* (1997). PTEN, a putative protein tyrosine phosphatase gene mutated in human brain, breast, and prostate cancer. *Science* **275**: 1943–1947.

Lin D, Edwards AS, Fawcett JP, Mbamalu G, Scott JD, Pawson T. (2000). A mammalian PAR-3–PAR-6 complex implicated in Cdc42/Rac1 and aPKC signalling and cell polarity. *Nat Cell Biol* **2**: 540–547.

Macara IG. (2004). Parsing the polarity code. *Nat Rev Mol Cell Biol* **5**: 220–231.

Mei R, Galipeau PC, Prass C, Berno A, Ghandour G, Patil N *et al.* (2000). Genome-wide detection of allelic imbalance using human SNPs and high-density DNA arrays. *Genome Res* **10**: 1126–1137.

Nagayama K, Kohno T, Sato M, Arai Y, Minna JD, Yokota J. (2007). Homozygous deletion scanning of the lung cancer genome at a 100-kb resolution. *Genes Chromosomes Cancer* **46**: 1000–1010.

Nannya Y, Sanada M, Nakazaki K, Hosoya N, Wang L, Hangaishi A *et al.* (2005). A robust algorithm for copy number detection using high-density oligonucleotide single nucleotide polymorphism genotyping arrays. *Cancer Res* **65**: 6071–6079.

Stevenson BR, Siliciano JD, Mooseker MS, Goodenough DA. (1986). Identification of ZO-1: a high molecular weight polypeptide associated with the tight junction (zonula occludens) in a variety of epithelia. *J Cell Biol* **103**: 755–766.

Suzuki A, Ohno S. (2006). The PAR–aPKC system: lessons in polarity. *J Cell Sci* **119**: 979–987.

Vizcaino AP, Moreno V, Lambert R, Parkin DM. (2002). Time trends incidence of both major histologic types of esophageal carcinomas in selected countries, 1973–1995. *Int J Cancer* **99**: 860–868.

Wodarz A, Näthke I. (2007). Cell polarity in development and cancer. *Nat Cell Biol* **9**: 1016–1024.

Yasui K, Imoto I, Fukuda Y, Pimkhaokham A, Yang ZQ, Naruto T *et al.* (2001). Identification of target genes within an amplicon at 14q12–q13 in esophageal squamous cell carcinoma. *Genes Chromosomes Cancer* **32**: 112–118.

Zhao X, Li C, Paez JG, Chin K, Jänne PA, Chen TH *et al.* (2004). An integrated view of copy number and allelic alterations in the cancer genome using single nucleotide polymorphism arrays. *Cancer Res* **64**: 3060–3071.

Zitzelsberger H, Hieber L, Richter H, Unger K, Briscoe CV, Peddie C *et al.* (2004). Gene amplification of atypical PKC-binding PARD3 in radiation-transformed neoplastic retinal pigment epithelial cell lines. *Genes Chromosomes Cancer* **40**: 55–59.

Supplementary Information accompanies the paper on the Oncogene website (http://www.nature.com/onc)

Journal of Cellular Physiology

Involvement of IQGAP3, a Regulator of Ras/ERK-Related Cascade, in Hepatocyte Proliferation in Mouse Liver Regeneration and Development

KOSHI KUNIMOTO,[1,2] HISASHI NOJIMA,[1] YUJI YAMAZAKI,[1] TOSHIKAZU YOSHIKAWA,[2] TAKESHI OKANOUE,[3] AND SACHIKO TSUKITA[1]*

[1]*Laboratory of Biological Science, Graduate School of Frontier Biosciences and Graduate School of Medicine, Osaka University, Osaka, Japan*

[2]*Molecular Gastroenterology and Hepatology, Graduate School of Medical Science, Kyoto Prefectural University of Medicine, Kyoto, Japan*

[3]*Department of Hepatology, Saiseikai Suita Hospital, Osaka, Japan*

The spatio-temporal regulation of hepatocyte proliferation is a critical issue in liver regeneration. Here, in normal and regenerating liver as well as in developing liver, we examined its expression/localization of IQGAP3, which was most recently reported as a Ras/Rac/Cdc42-binding proliferation factor associated with cell–cell contacts in epithelial-type cells. In parallel, the expression/localization of Rac/Cdc42-binding IQGAP1/2 was examined. IQGAP3 showed a specific expression in proliferating hepatocytes positive for the proliferating marker Ki-67, the levels of expressions of mRNAs and proteins were significantly increased in hepatocytes in liver regeneration and development. In immunofluorescence, IQGAP3 was highly enriched at cell–cell contacts of hepatocytes. IQGAP1 and IQGAP2 were exclusively expressed in Kupffer and sinusoidal endothelial cells, respectively, in normal, regenerating, and developing liver. The expression of IQGAP1, but not of IQGAP2, was increased in CCl_4-induced (but not in partial hepatectomy-induced) liver regeneration. Exclusive expression/localization of IQGAP3 to hepatocytes in the liver likely reflects the specific involvement of the IQGAP3/Ras/ERK signaling cascade in hepatocyte proliferation in addition to the previously identified signaling pathways, possibly by integrating cell–cell contact-related proliferating signaling events. On the other hand, the Rac/Cdc42-binding properties of IQGAP1/2/3 may be related to the distinct modes of remodeling due to the different strategies which induced proliferation of liver cells; partial hepatectomy, CCl_4 injury, or embryonic development. Thus, the functional orchestration of Ras and the Ras homologous (Rho) family proteins Rac/Cdc42 likely plays a critical role in liver regeneration and development.

J. Cell. Physiol. 220: 621–631, 2009.

The spatio-temporal regulation of hepatocyte proliferation is critical for liver cell biology and also for clinical therapy of liver regeneration, such as that in acute liver failure and cirrhosis. In the normal adult liver, most hepatocytes are in a quiescent state and a few hepatocytes turn over very slowly, so that the liver size is tightly regulated (Michalopoulos and DeFrances, 1997; Fausto, 2000; Fausto et al., 2006; Michalopoulos, 2007). In contrast, hepatocyte proliferation is prominent in particular periods such as liver regeneration and embryonic liver development. Although a series of studies on the mechanisms regulating cell proliferation have been performed in animals subjected to partial hepatectomy or chemical injury, using wild-type and various transgenic and knockout mouse models, the similarities and differences between mechanistic cell signals in liver regeneration and in embryonic liver development are not well understood (Zhao and Duncan, 2005). Following partial hepatectomy or acute toxic liver injury in rodents, the liver restores the mass to its original size within a few weeks. In the 1960s, it was shown in rats that during liver regeneration, hepatocytes were actively engaged in DNA synthesis, and it was estimated that 70–90% of hepatocytes underwent at least one round of cell division during this process.

The proliferation process of differentiated hepatocytes may pass through several phases, such as priming phases by cytokines, followed by cell-cycle progression phases by growth factors and metabolic demands. Hepatocytes need to be primed by cytokines such as TNF and IL-6 in addition to other agents that prevent cytotoxicity. Among numerous transcription factors, notably NF-kappaB and STAT3 play major roles in the initiation of liver regeneration. Progression through the cell cycle beyond the initiation phase requires growth factors such as HGF, TGF-α, and EGF, so that ERKs and cyclin D1 probably establish the stage at which replication becomes growth factor independent and autonomous (Talarmin et al.,

Koshi Kunimoto and Hisashi Nojima contributed equally to this work.

Additional Supporting Information may be found in the online version of this article.

Contract grant sponsor: Ministry of Education, Science and Culture of Japan;
Contract grant sponsor: Ministry of Education, Culture, Sports, Science and Technology of Japan.

*Correspondence to: Sachiko Tsukita, Laboratory of Biological Science, Graduate School of Frontier Biosciences and Graduate School of Medicine, Osaka University, Yamadaoka 2-2, Suita, Osaka 565-0871, Japan. E-mail: atsukita@biosci.med.osaka-u.ac.jp

Received 16 February 2009; Accepted 23 March 2009
Published online in Wiley InterScience (www.interscience.wiley.com), 18 May 2009.
DOI: 10.1002/jcp.21798

1999; Frémin et al., 2007; Michalopoulos, 2007). On the other hand, although signals in the spatio-temporal regulation of hepatocyte proliferation in embryonic liver development have been noted, such as HGF- and Notch-related signaling pathways as well as HNF4 signaling (Parviz et al., 2003; Lemaigre and Zaret, 2004), the complete correlative view of the signaling pathways of liver regeneration and development remains to be elucidated. At this stage, it is important to integrate information with respect to multi-sided signaling pathways. The role of small GTP-binding proteins that is generally the focus in the spatio-temporal regulation of cell adhesion, proliferation, and motility is currently lacking in hepatocyte biology.

Most recently, we reported that IQGAP3, a Ras/Rac/Cdc42-binding protein, was expressed specifically in proliferating cells in culture and also in vivo, such as in transit-amplifying cells of the small intestine (Wang et al., 2007; Nojima et al., 2008). In culture, when forcibly expressed, it drove cell proliferation by regulating Ras/ERK signaling pathways. Here we found that the expression of IQGAP3 was confined to proliferating hepatocytes, the number of which was very limited in normal adult liver where non-proliferating hepatocytes dominated. The expression of IQGAP3 was highly induced in the liver regeneration process due to partial hepatectomy and CCl_4 injury and was also induced in the liver development process, suggesting that the novel IQGAP3/Ras/ERK-related signaling was involved in vivo in hepatocyte proliferation. On the other hand, IQGAP1/2 with binding affinity to Rac and Cdc42 showed distinct localization in Kupffer and sinusoidal endothelial cells, respectively (Li et al., 2000; Sugimoto, 2001; Noritake et al., 2005; Emadali et al., 2006; Brandt and Grosse, 2007; Brandt et al., 2007; Schmidt et al., 2008). The findings were discussed with special reference to the Ras-mediated critical role of IQGAP3 in hepatocyte proliferation and to the Rac- and Cdc42-mediated roles of IQGAP1/2/3 in Kupffer and sinusoidal endothelial cells and hepatocytes, respectively, in tissue remodeling due to liver regeneration and embryonic liver development. Since IQGAP1/2/3 were reported as the cell–cell contact-related proteins, they might well play critical roles as interfaces between cell–cell interaction and cell proliferation/remodeling.

Materials and Methods

Treatment of animals

C57BL/6J mice, aged 2–12 weeks, and pregnant mice (day 15, day 18) were purchased and housed in a specific pathogen-free facility at Osaka University Medical School, and all animal experiments were carried out in accordance with protocols approved by the Osaka University Medical School Animal Care and Use Committee.

Antibodies

Rabbit anti-mouse IQGAP1, 2, and 3 polyclonal antibodies (pAbs) were used as previously described (Nojima et al., 2008). Guinea pig anti-mouse afadin pAb was generated using amino acids 1447–1822 of afadin (Katsuno et al., 2008). Rat anti-mouse BM8 (F4/80) monoclonal antibody (mAb) (BM4007S; Acris, Herford, Germany), cy3-conjugated mouse anti-glial fibrillary acidic protein (GFAP) mAb (G-A-5; Sigma-Aldrich, St. Louis, MO), cy3-conjugated mouse anti-α-smooth-muscle actin mAb (1A4; Sigma), rat anti-mouse ICAM-1 (CD54) mAb (YN1/1.7.4; Biolegend, San Diego, CA), rat anti-Ki-67 mAb (TEC-3; DakoCytomation, Glostrup, Denmark), rabbit anti-mouse albumin pAb (RAM/Alb/7S; Nordic Immunology, Tilburg, The Netherlands), rat anti-mouse PECAM-1 (CD31) mAb (MEC 13.3; BD Biosciences Pharmingen, San Diego, CA), PE-conjugated rat anti-mouse CD45 mAb (12-0451; eBioscience, San Diego, CA), PE-conjugated rat anti-mouse CD11b mAb (12-0112; eBioscience), and rabbit anti-mouse GAPDH pAb (G9545; Sigma) were obtained from commercial sources. These antibodies were diluted according to the manufacturer's instructions.

Two-thirds partial hepatectomy and CCl_4 treatment for mice

Eight-week-old mice were subjected to two-thirds partial hepatectomy (modified Higgins & Anderson method) or CCl_4 (1.6 ml/kg intraperitoneal injection diluted with mineral oil) administration to induce liver regeneration (Higgins and Anderson, 1931; Farber and Gerson, 1984). They were then sacrificed at each time point after partial hepatectomy or CCl_4 injury. The regenerating livers were harvested and used for total RNA isolation, protein extraction, and immunohistostaining.

Immunoblotting

Liver samples were lysed with SDS–PAGE sample buffer, sonicated and boiled, and used as total liver cell lysates. Protein samples were separated by SDS–PAGE and transferred onto nitrocellulose or PVDF membranes, and blotted with appropriate antibodies.

Immunofluorescence microscopy

Mouse liver tissues were frozen using liquid nitrogen. Frozen sections, approximately 5 μm thick, were immunostained as previously described (Nojima et al., 2008).

Quantitative real-time RT-PCR

Total RNA was prepared from each liver sample and the cDNA was reverse transcribed and used as a template for quantitative real-time PCR analysis using a QuantiTect SYBR Green PCR kit (Qiagen, Hilden, Germany), as described previously (Kubo et al., 2008). The primer sets used for quantitative real-time RT-PCR analysis of IQGAP mRNA in liver cells were as follows: mouse IQGAP1, forward primer (5′-ACGCTGATCAGAGCAAAG-AGAGAA-3′) and reverse primer (5′-GAGATTCCTAAGG-CAAACCTCTGG-3′); mouse IQGAP2, forward primer (5′-CAAACAGAGAGCGTGGTCAA-3′) and reverse primer (5′-TCGGAACCAGGACTGAATCT-3′); mouse IQGAP3, forward primer (5′-CCTGGAACAGCTGACTTCAG-3′) and reverse primer (5′-CCACACAGCCTGGAGCATAG-3′); mouse GAPDH, forward primer (5′-AAGGTGGTGAAGCAGGCA-TCTGAG-3′) and reverse primer (5′-GGAAGAGTGGGA-GTTGCTGTTGAAGTC-3′). GAPDH was used as an internal control. The mean and SD for each time point were calculated.

Results

Specific localization of IQGAP1/2/3 in Kupffer cells, sinusoidal endothelial cells, and proliferating hepatocytes, respectively, in normal adult liver

Based on previous results that, when expressed, IQGAP3, but not IQGAP1 or IQGAP2, showed a remarkable effect on proliferation through the Ras/ERK signaling cascade, we examined the role of IQGAP3 in hepatocyte proliferation from the viewpoint of liver development and regeneration (Nojima et al., 2008). At first, we immunofluorescently examined the distinct localization patterns of IQGAP1/2/3 in 12-week-old adult mouse liver (Fig. 1). IQGAP1/2/3 showed different patterns of localization in the liver. The IQGAP1 signal was mainly detected in rather small, irregularly shaped, scattered cells along the sinusoid, which were positive for the Kupffer cell marker BM8 (Schaller et al., 2002; Peng and Murr, 2007), but was not detected in other types of cells such as GFAP-positive hepatic stellate cells or αSMA-positive activated stellate cells (data not shown) (Hautekeete and Geerts, 1997). The IQGAP2 signal was detected in sinusoidal lining cells, positive for ICAM-1 (CD54) (Couvelard et al., 1996).

In sharp contrast, the IQGAP3 signal was usually hardly detected, but was occasionally detected in hepatocytes (0–1 cells/hepatic lobule) positive for Ki-67, a general

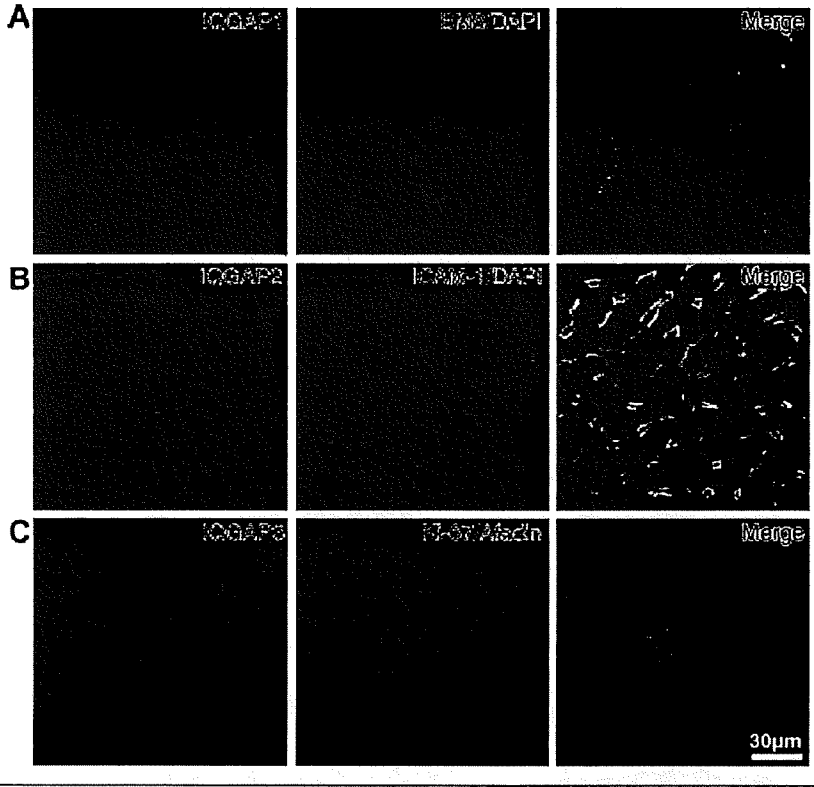

Fig. 1. Specific localization of IQGAP1/2/3 in Kupffer cells, sinusoidal endothelial cells, and proliferating hepatocytes, respectively, in normal adult liver. Immunofluorescence micrographs of normal adult liver stained for IQGAP1 (A), IQGAP2 (B), and IQGAP3 (C). A: Immunofluorescence for IQGAP1 (green), co-stained for Kupffer cell marker BM8 (red) and DAPI (blue). The IQGAP1 signal was detected in rather small, irregularly shaped, scattered cells along the sinusoid, which were positive for Kupffer cell marker BM8. B: Immunofluorescence for IQGAP2 (green), co-stained for ICAM-1 (CD54) (red) and DAPI (blue). The IQGAP2 signal was detected in sinusoidal lining cells, positive for ICAM-1 (CD54). C: Immunofluorescence micrographs for IQGAP3 (green), co-stained for Ki-67 (red) and afadin (blue). The IQGAP3 signal was occasionally detected in hepatocytes (0–1 cell/hepatic lobule), which were also positive for Ki-67.

proliferation marker (Gerlach et al., 1997). The positive IQGAP3 signal was detected just around the cell–cell contacts with weak cytoplasmic signals. These findings revealed the distinct localization of IQGAP1/2/3 in Kupffer cells, sinusoidal endothelial cells, and hepatocytes, respectively, and IQGAP3 localization was specifically associated with proliferating hepatocytes, but not with non-proliferating hepatocytes in adult liver. In addition, due to the clear staining of IQGAP3 in the cell–cell contacts of hepatocytes, which silhouetted the hepatocytes, IQGAP3 was likely an unique proliferation marker which showed the whole cell outline of proliferating cells.

Specific immunofluorescence signals of IQGAP1/2/3 in embryonic proliferating mouse hepatoblasts and hepatocytes

Next, since IQGAP3 immunofluorescence signals seemed to be specifically associated with Ki-67-positive proliferating cells in normal liver, we followed the immunofluorescence of IQGAP3 during the establishment of tissue architecture in the developing liver of mice from embryonic day 15 (E15) to postnatal day 28 (P28) (Fig. 2). At E15, E18, P1, and P14, ~85%, 70%, 70%, and 10% of total liver cells were Ki-67-positive, suggesting that they were proliferating. Many embryonic hematopoietic liver cells were small-shaped and IQGAP3- and Ki-67-positive with the exception that some cells were Ki-67-positive but IQGAP3-negative at E15 when we could not recognize normal adult architecture of liver. Since Ki-67 and IQGAP3 double-positive cells immunofluorescently showed an affinity to mouse albumin, these double-positive cells were likely hepatoblasts. On the other side, Ki-67-positive but IQGAP3-negative cells were not positive for mouse albumin, suggesting that they were non-hepatoblastic cells (data not shown).

In liver tissue architecture at E18 and P1 when normal liver architecture was partly formed, the number of Ki-67 and IQGAP3 double-positive proliferating hepatocytes decreased. When the liver architecture was almost established around P14 with hepatocytes of rather small size, and the central vein region as well as the portal vein region was established, as shown by afadin staining (Figs. 2 and 4), the signals of IQGAP3 and Ki-67 significantly decreased. At P28, the mouse liver architecture was matured and almost the same as that of 12-week-old mouse liver, occasionally with Ki-67 and IQGAP3 double-positive large cells (1–2 cells/lobule) scattered liver lobules. Additionally, we followed immunofluorescence signals for IQGAP3 and Ki-67 up to a 50-week-old mouse liver and found the similar staining patterns to those in 12-week-old mouse liver (data not shown). Thus, it was noted that IQGAP3 had specifically marked Ki-67-positive proliferating hepatocytes, silhouetting the outlines of proliferating hepatocytes. These results showed that IQGAP3 was more useful as a specific proliferation marker for hepatocytes, than Ki-67.

To characterize the patterns of the spatio-temporal proliferation of hepatocytes in tissue architecture, we

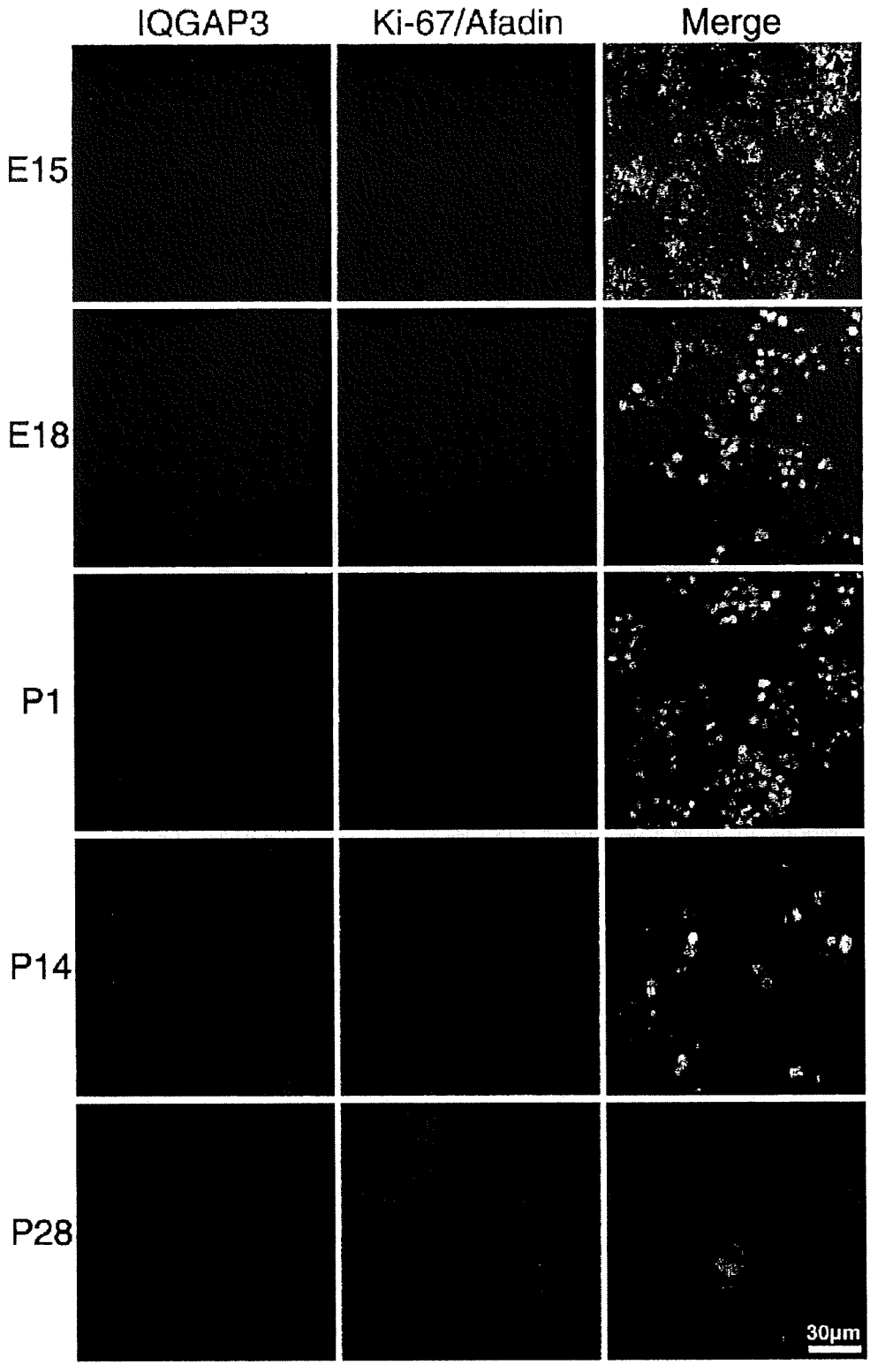

Fig. 2. Differentiation-dependent changes of IQGAP3 expression in hepatoblasts and hepatocytes. Triple-stained immunofluorescence micrographs of IQGAP3 (green), Ki-67 (red), and afadin (blue) during development, at E15, E18, P1, P14, and P28. At E15, E18, P1, and P14, ~85%, 70%, 70%, and 10% of total liver cells were Ki-67-positive. At E15, all hepatoblastic cells were small and positive for IQGAP3 (green) and Ki-67 (red). Non-hepatoblastic cells were Ki-67-positive but IQGAP3-negative. At E18 and P1, when normal liver architecture was partly formed, the number of Ki-67 and IQGAP3 double-positive proliferating hepatocytes decreased. At P14, the liver architecture was almost established with hepatocytes of rather small size, and the central vein region as well as the normal portal vein region was established, as shown by afadin staining. The signals of IQGAP3 and Ki-67 significantly decreased. At P28, the mouse liver architecture was matured with IQGAP3 and Ki-67 double-positive large cells only occasionally (1–2 cell/lobule) scattered in liver lobules.

examined the immunofluorescence for IQGAP1 and IQGAP2 in the developing liver of mice from E15 to P14. We found that the immunofluorescence images were quite distinct from those for IQGAP3. Consistent with normal liver, immunofluorescence signals for IQGAP1 and IQGAP2 were detected specifically in Kupffer cells and endothelial cells, respectively, in any developmental stages (Figs. 3 and 4), when Kupffer cells were identified by BM8 signals (Fig. 3A) and endothelial cells were identified by PECAM-1 signals (data not shown), whose distribution patterns were deduced from afadin staining (Fig. 4); however, IQGAP1 signals were also detected from E18 to P1 in small round cells, which were positive for a pan-hematopoietic cell marker, CD45, and for a monocyte-specific marker, CD11b, believed to be destined for at least partly pre-Kupffer-like properties (Fig. 3B). As a result, during development, Kupffer cells were lined along sinusoids, thus encircling the islands of hepatocytes, which were proliferating, as shown by the positive signals for Ki-67 (P1 of Fig. 2). The relationship between sinusoids and the islands of hepatocytes in developing stages was more evident by IQGAP2 immunofluorescence signals (P1 of Fig. 4). After P7, as revealed by the immunofluorescence of IQGAP1 and IQGAP2, the hepatocytes were more finely arranged in more mature states. Thus, IQGAP2 showed immunofluorescence patterns, which reflected the maturating stages in accordance with the step-wise maturation mechanism of liver tissue architecture.

Specific increase of IQGAP1/2/3 in the levels of mRNAs and proteins in developing embryonic liver and also in regenerating liver due to partial hepatectomy and CCl_4 injury

Since immunofluorescence signals for IQGAP1/2/3 changed during embryonic liver development, the expression of IQGAP1/2/3 was examined in the total liver at the level of mRNA and protein by real-time RT-PCR and immunoblotting, respectively (Fig. 5A). Total liver samples were collected from four animals at each time point: E15, E18, P1, P7, P14, P28, P42, and P56. Total mRNAs and proteins were isolated from each sample, which were subsequently subjected to real-time RT-PCR and immunoblotting to examine the levels of IQGAP1/2/3 and GAPDH (internal control). Consistently, the mRNA and protein levels of IQGAP3 were high in the embryonic stages and also after postnatal stages until 2 weeks, and the levels subsequently fell markedly. The mRNA and protein levels of IQGAP1 also decreased after P7, whereas changes in the levels of IQGAP2 showed complementary patterns to those of IQGAP3.

Next, considering that hepatocyte proliferation was associated with the expression of IQGAP3 in normal adult and embryonic developing liver, our attention was drawn to the expression of IQGAP3 in liver regeneration. For this purpose, hepatocyte proliferation was evoked by partial hepatectomy and CCl_4 injury. The levels of mRNAs and total proteins of IQGAP1/2/3 were examined by real-time RT-PCR and immunoblotting, respectively (Fig. 5B). After treatment with partial hepatectomy or CCl_4 injury, total liver samples were collected from three animals at each time point: 0 (pre), 1, 2, 3, 4, 6, 8, 10, and 14 days. Total mRNAs and proteins were isolated from each sample, subsequently subjected to real-time RT-PCR and immunoblotting to examine the levels of IQGAP1/2/3 and GAPDH (internal control). Although changes in the levels of IQGAP2 were not apparent, IQGAP1 and IQGAP3 showed significant changes in their expression levels. The expression levels of mRNAs and proteins of IQGAP3 were transiently increased during day 2–day 4 (2d–4d) after partial hepatectomy and CCl_4 injury. This timing of increased IQGAP3 expression is highly consistent with that of hepatocyte proliferation during liver regeneration, as generally reported (Fausto et al., 2006; Michalopoulos, 2007). In contrast, expression levels of mRNAs and proteins of IQGAP1 showed an increase during day 1–day 4 (1d–4d) after CCl_4 injury, but not after partial hepatectomy, suggesting the different modes of liver regeneration between partial hepatectomy and CCl_4 injury.

Immunofluorescence microscopic examination of the localization of IQGAP1/2/3 in regenerating liver induced by partial hepatectomy and CCl_4 injury

Changes in the expression levels of mRNAs and proteins of IQGAP1 and IQGAP3 led us to examine the immunofluorescence intensities of IQGAP1/2/3 in liver regeneration (Figs. 6, 7, and S1–4). After treatment with partial hepatectomy or CCl_4 injury, total liver samples were collected from three animals at each time point: 1, 2, 3, 4, and 14 days. In all cases, IQGAP1/2/3 were specifically associated with Kupffer cells, sinusoidal endothelial cells, and proliferating hepatocytes, respectively, similar to the normal liver (Fig. 1). IQGAP3 signals were always detected in proliferating hepatocytes with a positive signal for Ki-67 (Figs. 6 and 7). The number of IQGAP3-positive proliferating cells was highly increased during 2d–4d after partial hepatectomy and CCl_4 injury. In these cells, IQGAP3 was dominantly enriched in the plasma membranes of hepatocytes without immunofluorescence signals detected in other types of cells than hepatocytes. The IQGAP1 signal was confined to Kupffer cells positive for BM8 (Figs. S1 and S3). As for the basis for the increase of IQGAP1 expression in the levels of mRNAs and proteins after CCl_4 injury, strong IQGAP1 signals were detected in damaged areas of the liver, in contrast, this type of damage was not induced by partial hepatectomy without increased levels of IQGAP1. These results suggested the repair-dependent increase of the expression level of IQGAP1, consistent with previous reports on Kupffer cells accumulated in the damaged area (Edwards et al., 1993; Badger et al., 1996). Except for the damaged area with no IQGAP2 specific immunofluorescent signal after CCl_4 injury, the intensity and localization of the IQGAP2 signal were not changed in liver regeneration, markedly detectable in sinusoidal endothelial cells (Figs. S2 and S4).

Discussion

In the present study, we found the unique pattern of the respective expression/localization of IQGAP1/2/3 in the liver in relation to liver regeneration and development. Among them, IQGAP3, but not IQGAP1 or IQGAP2, was dominantly expressed in hepatocytes and its expression levels of mRNAs and proteins showed a critical correlation with hepatocyte proliferation in liver regeneration. The expression of IQGAP1/2 was detected in Kupffer and sinusoidal endothelial cells, respectively. These findings were partly inconsistent with the previous statements that IQGAP1 and/or IQGAP2 were expressed in hepatocytes (Emadali et al., 2006; Schmidt et al., 2008). However, further studies on these points are required in future to conclusively determine the specific signals in hepatocytes, since for rather weak signals in tissue, several points are needed to be critically examined with respect to conditions for immunostaining.

IQGAP1/2/3 are totally considered to play a role as an interface between the plasmalemmal scaffolds and signaling pathways through small GTP-binding proteins (Noritake et al., 2005; Brandt et al., 2007; Wang et al., 2007; Nojima et al., 2008). They are reportedly associated with the cell–cell contact region and bind to dominant active forms of Rac and Cdc42, among which IQGAP3 is shown to bind to Ras. In this respect, it was reported that IQGAP1 might be integrated in cell–cell adhesion through linkage to the cadherin–catenin and/or nectin–afadin system (Yamada et al., 2006). Hence, it is plausible that at least some IQGAP1/2/3 at a particular time might play a role in

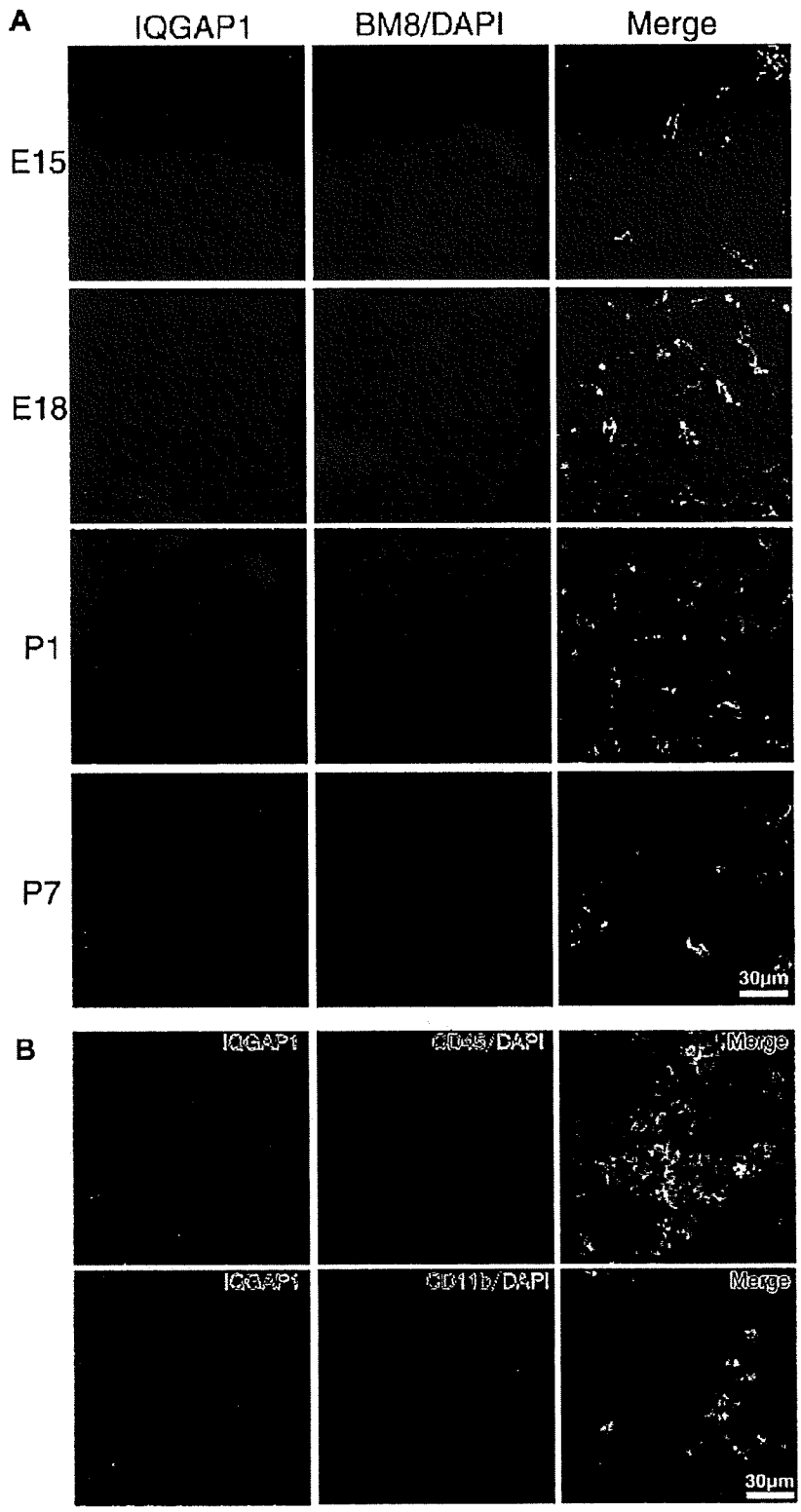

Fig. 3. Immunofluorescence pattern of IQGAP1 proteins in the developing liver. A: Triple-stained immunofluorescence micrographs of IQGAP1 (green), BM8 (red), and DAPI (blue) during development, at E15, E18, P1, and P7. B: Triple-stained immunofluorescence micrographs of IQGAP1 (green), CD45 (red), and DAPI (blue) at P1, and of IQGAP1 (green), CD11b (red), and DAPI (blue) at E18. IQGAP1 showed immunofluorescence signals, specifically in BM8-positive Kupffer cells in any developmental stage (A); however, IQGAP1 signals were also detected from E18 to P1 in small round cells, positive for a pan-hematopoietic cell marker, CD45, and for a monocyte-specific marker, CD11b, believed to be destined for at least partly pre-Kupffer-like properties (B).

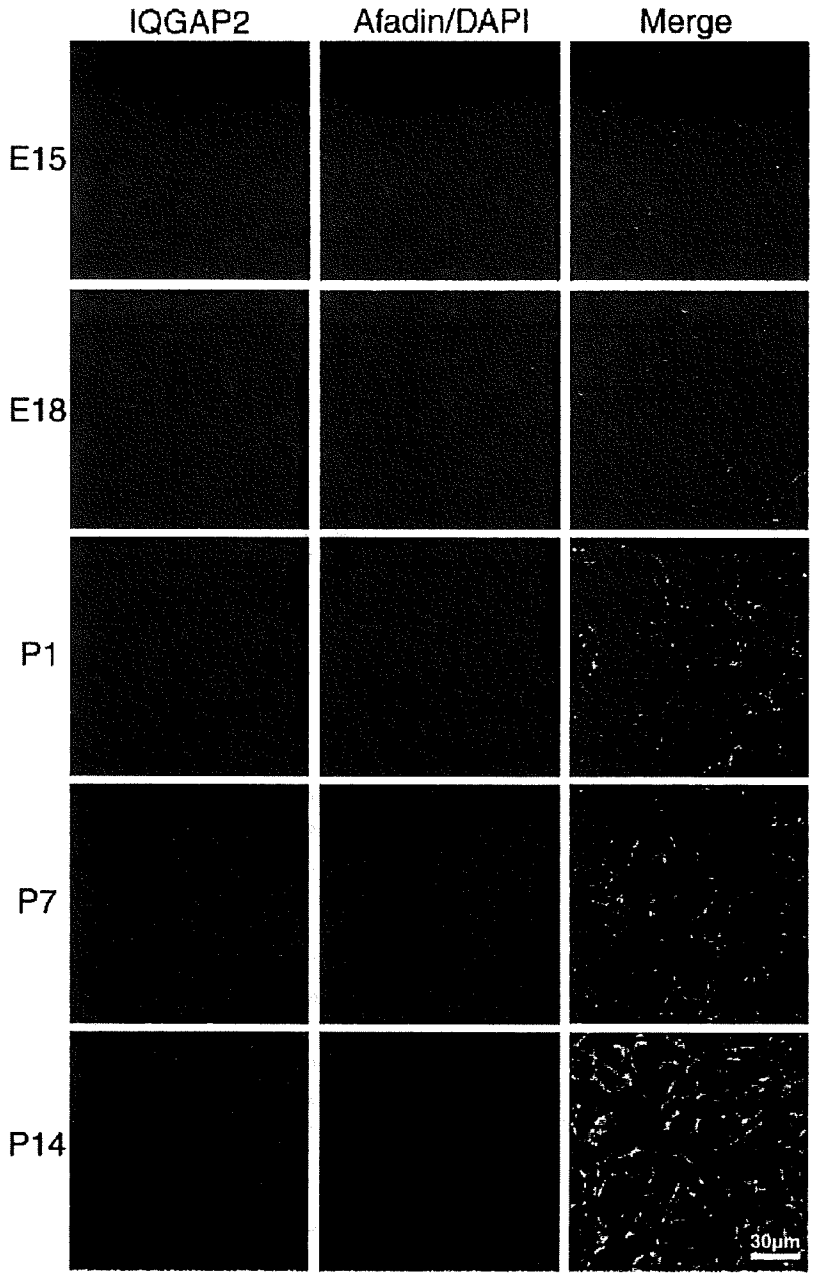

Fig. 4. Immunofluorescence pattern of IQGAP2 proteins in the developing liver. Triple-stained immunofluorescence micrographs of IQGAP2 (green), afadin (red), and DAPI (blue) during development, at E15, E18, P1, P7, and P14. IQGAP2 showed specifically in endothelial cells, whose distribution patterns were deduced from afadin staining in any developmental stage. The relationship between sinusoids and islands of hepatocytes in developing stages was evident from IQGAP2-immunofluorescence signals. After P7, as revealed by immunofluorescence for IQGAP2, hepatocytes were more finely arranged in more mature states.

integrating cell–cell contact-related information with cell signaling events in cell movement and proliferation. Thus, it is an indispensable step to compare the expression/localization of IQGAP1/2/3 in normal, developing, and regenerating liver.

From more hepatologically oriented aspects, the current research stage demands the collection of various types of information on the signaling cascades involved in liver regeneration and development, since several types of signaling pathways, such as priming by cytokines and cell-cycle progression by growth factors, have been reported to be involved, but not yet elucidated, especially for diagnostic strategies for liver regeneration in disease and liver transplantation (Fausto et al., 2006; Michalopoulos, 2007). In this respect, the contribution of IQGAP1/2/3 to liver regeneration and development seemed marked. Taking the previous cell level analysis that IQGAP3 promoted cell proliferation through the Ras/ERK pathway with the present finding that the expression level of IQGAP3 at cell–cell contacts of hepatocytes was increased during the proliferating phase, one of the most potent future issues is to identify the cell

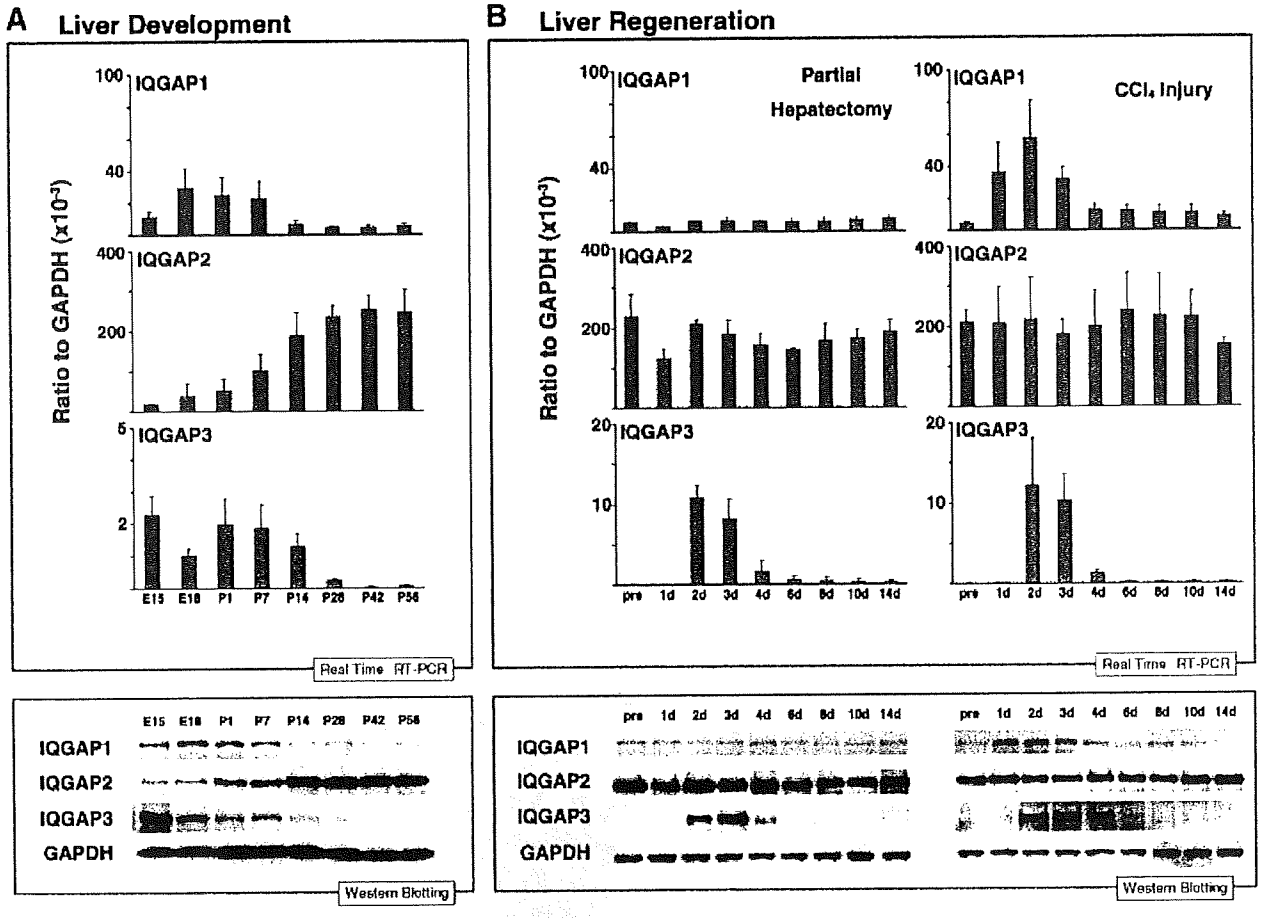

Fig. 5. Specific increase of IQGAP1/2/3 in the levels of mRNAs and proteins in developing embryonic liver and also in regenerating liver due to partial hepatectomy and/or CCl_4 injury. A: Real-time RT-PCR and immunoblotting of the developing liver for IQGAP1/2/3. Total liver samples were collected from four animals at E15, E18, P1, P7, P14, P28, P42, and P56. Total mRNAs and proteins were isolated from each sample and examined. Consistently, mRNA and protein levels of IQGAP3 were high in embryonic stages and also after postnatal stages until 2 weeks, and then fell markedly. The mRNA and protein levels of IQGAP1 also decreased after P7, whereas changes in the levels of IQGAP2 showed complementary patterns to those of IQGAP3. B: Real-time RT-PCR and immunoblotting of the regenerating liver induced by partial hepatectomy and by CCl_4 injury are shown. After partial hepatectomy or CCl_4 injury, total liver samples were collected from three animals at 0 (pre), 1, 2, 3, 4, 6, 8, 10, and 14 days. Total mRNAs and proteins were isolated from each sample and examined. Although changes in the levels of IQGAP2 were not apparent, IQGAP1 and IQGAP3 showed significant changes in their expression levels. The expression levels of mRNAs and proteins of IQGAP3 were transiently increased during day 2–day 4 (2d–4d) after partial hepatectomy and CCl_4 injury. This timing of increased IQGAP3 expression is highly consistent with that of hepatocyte proliferation during liver regeneration, as generally reported. In contrast, the expression levels of mRNAs and proteins of IQGAP1 showed an increase during day 1–day 4 (1d–4d) after CCl_4 injury, but not after partial hepatectomy, suggesting different modes of liver regeneration between partial hepatectomy and CCl_4 injury.

density-sensing units at cell–cell contacts in association with IQGAP3 (Nojima et al., 2008); however, it is also necessary to elucidate the mechanism by which IQGAP3 was processed to decrease the expression levels of mRNAs and proteins (Fig. 5). Phenomenologically, IQGAP3 was once up-regulated 2d–4d after partial hepatectomy and CCl_4 injury associated with the transient hepatocyte proliferation. Then, IQGAP3 was down-regulated to the basal level when hepatocyte proliferation dropped to nearly zero (Figs. 6 and 7). Since the mechanism behind this decrease of hepatocyte proliferation seemed to be related to contact inhibition of cell growth, the decrease in the expression level of IQGAP3 was plausible as a cause or a result of contact inhibition of cell proliferation, the detailed molecular mechanism of which is a future issue.

In the present study, IQGAP1 was up-regulated during tissue repair after CCl_4 injury and also during tissue development (Figs. 3, 5, and S3). Since IQGAP1 was dominantly expressed in Kupffer cells in the normal adult and also in the regenerating and developing liver with binding characteristics to Rac and Cdc42, IQGAP1 likely contributed to these activities, possibly through Rac- and/or Cdc42-signaling pathways in Kupffer cells. The similar roles of IQGAP1 in cell–cell adhesion and motility as suggested in Kupffer cells might possibly be attributed to IQGAP2 and IQGAP3 in sinusoidal endothelial cells and in hepatocytes, respectively, due to their binding affinities to Rac1 and Cdc42 (Noritake et al., 2005; Brandt et al., 2007; Nojima et al., 2008). If this is the case, in hepatocytes in which Ras-binding IQGAP3 was expressed, IQGAP3 might integrate the signals of Ras with those of Rac1 and Cdc42, possibly leading to effective coordination of these signaling processes for cell proliferation and tissue remodeling.

In the liver, IQGAP1 was dominantly expressed in non-epithelial-type Kupffer cells, the number of which changed according to their needs for tissue repair and tissue genesis,

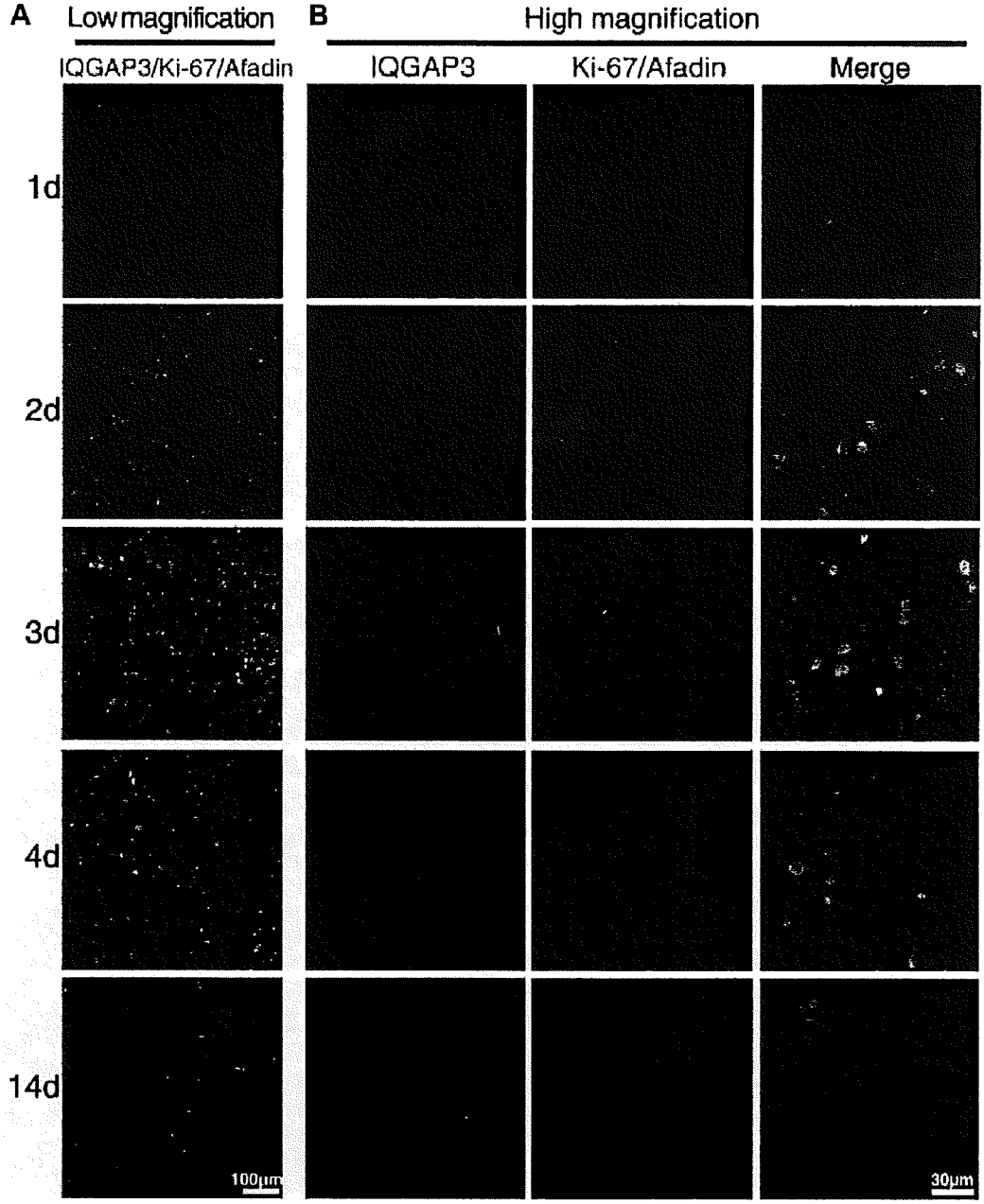

Fig. 6. Immunofluorescence micrographs of the localization of IQGAP3 in regenerating liver induced by partial hepatectomy. A,B: Triple-stained immunofluorescence micrographs of IQGAP3 (green), Ki-67 (red), and afadin (blue) during regeneration, at 1, 2, 3, 4, and 14 days after partial hepatectomy. High magnification view (A) and low magnification view (B). Signals for IQGAP3 were always detected in proliferating hepatocytes with a positive signal for Ki-67. The number of IQGAP3-positive proliferating cells was highly increased during 2d–4d after partial hepatectomy, and was decreased at 14 days. In these cells, IQGAP3 was dominantly enriched in the plasma membranes of hepatocytes without the immunofluorescence signal detected in other types of cells than hepatocytes.

thus possibly leading to cell proliferation-dependent changes in the expression levels of mRNAs and proteins of IQGAP1; however, the protein concentration of IQGAP1 in a single Kupffer cell was judged as approximately equal between normal and regenerating liver, based on immunofluorecence intensities (Fig. 1, S1, and S3). In the situation in which Kupffer cells seemingly proliferated, we could not detect a positive signal of IQGAP3 in Kupffer cells in spite of the positive signal of Ki-67, suggesting that IQGAP3 might not play a major role in driving cell proliferation in Kupffer cells (Fig. S3). The cell type-dependent contribution of IQGAP3 to cell proliferation in vivo, as exemplified in the liver, seems to add a new view to the functional aspects of IQGAP3 in cell proliferation.

The distinct localization patterning of IQGAP1/2/3 in the liver is contrasted to that in the small intestine, where it was reported that IQGAP1 was expressed in all types of cells,

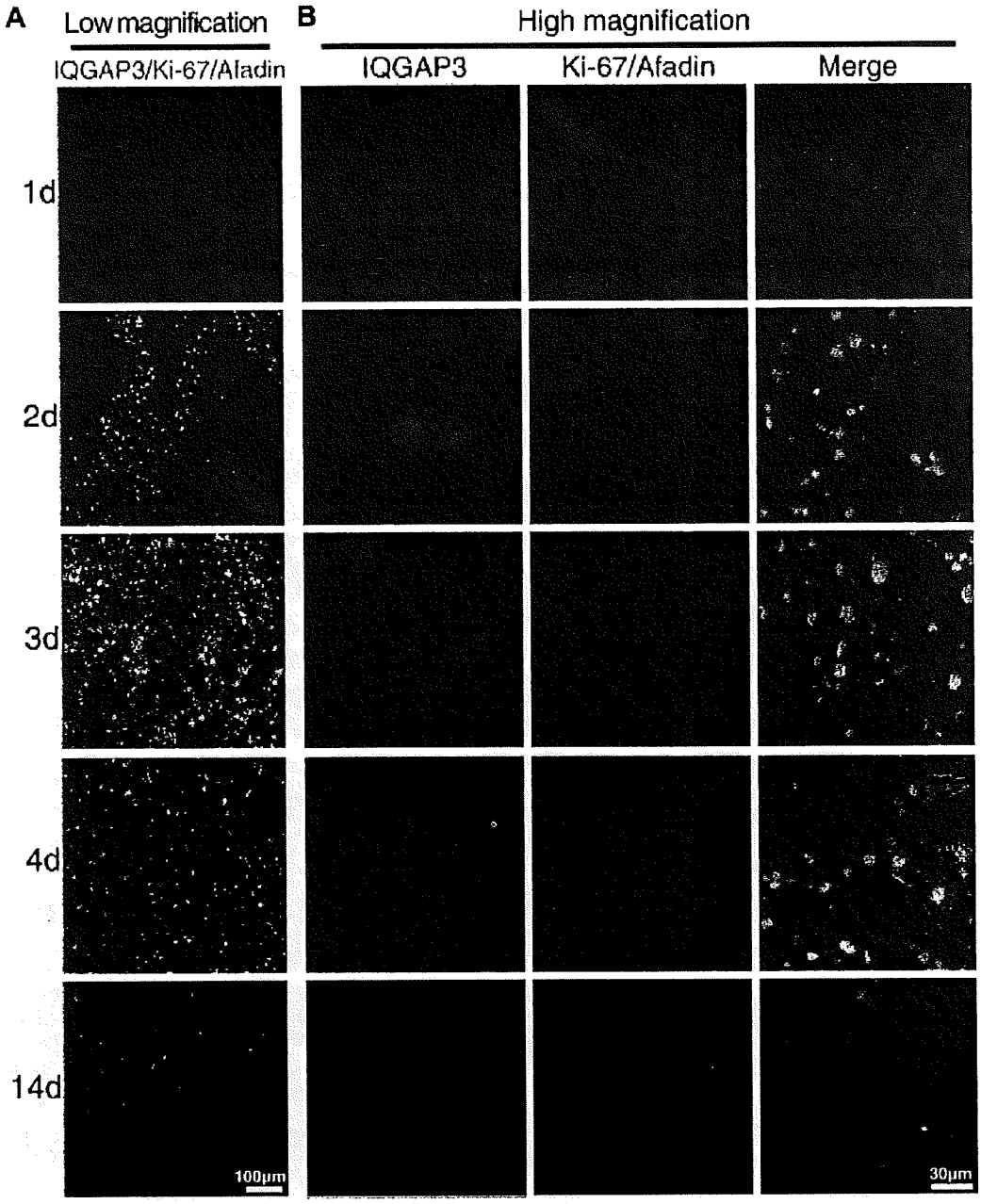

Fig. 7. Immunofluorescence micrographs of the localization of IQGAP3 in regenerating liver induced by CCl_4 injury. A,B: Triple-stained immunofluorescence micrographs of IQGAP3 (green), Ki-67 (red), and afadin (blue) during regeneration, at 1, 2, 3, 4, and 14 days after CCl_4 injury. High magnification view (A) and low magnification view (B). Signals for IQGAP3 were always detected in proliferating hepatocytes with a positive signal for Ki-67. The number of IQGAP3-positive proliferating cells was highly increased during 2d–4d after CCl_4 injury, and was decreased at 14 days. In these cells, IQGAP3 was dominantly enriched in the plasma membranes of hepatocytes without the immunofluorescence signal detected in other types of cells than hepatocytes.

whereas IQGAP2 and IQGAP3 were confined to villous and cryptic epithelial cells, respectively (Nojima et al., 2008). The distinct and/or shared roles of IQGAP1/2/3 in vivo in various types of cells might be related to variations in the balance of cell differentiation, motility, and adhesion, thus related to the specific morphogenesis of each organ.

It is likely that the signaling pathways used in liver regeneration might not be simple, but rather complex, combining various signaling pathways (Fausto et al., 2006; Michalopoulos, 2007). The IQGAP3-related signaling pathway may be one of the complex signaling routes involved in liver regeneration. The findings of the contribution of Ras-, Rac-, and Cdc42-binding IQGAP3 to liver regeneration possibly suggest the integration of cell proliferation with cell–cell adhesion and cell motility-related events to organize tissue genesis in a pre-existent tissue constitution of hepatocytes in the liver. Further

studies along these lines will lead to better understanding of the mechanism of liver regeneration with respect to developing a new strategy for liver therapy.

Acknowledgments

This study was supported in part by a Grant-in-Aid for Creative Scientific Research from the Ministry of Education, Science and Culture of Japan and Grant-in-Aid for Cancer Research from the Ministry of Education, Culture, Sports, Science and Technology of Japan, to Sachiko Tsukita.

Literature Cited

Badger DA, Sauer JM, Hoglen NC, Jolley CS, Sipes IG. 1996. The role of inflammatory cells and cytochrome P450 in the potentiation of CCl4-induced liver injury by a single dose of retinol. Toxicol Appl Pharmacol 141:507–519.

Brandt DT, Grosse R. 2007. Get to grips: Steering local actin dynamics with IQGAPs. EMBO Rep 8:1019–1023.

Brandt DT, Marion S, Griffiths G, Watanabe T, Kaibuchi K, Grosse R. 2007. Dia1 and IQGAP1 interact in cell migration and phagocytic cup formation. J Cell Biol 178:193–200.

Couvelard A, Scoazec JY, Dauge MC, Bringuier AF, Potet F, Feldmann G. 1996. Structural and functional differentiation of sinusoidal endothelial cells during liver organogenesis in humans. Blood 87:4568–4580.

Edwards MJ, Keller BJ, Kauffman FC, Thurman RG. 1993. The involvement of Kupffer cells in carbon tetrachloride toxicity. Toxicol Appl Pharmacol 119:275–279.

Emadali A, Muscatelli-Groux B, Delom F, Jenna S, Boismenu D, Sacks DB, Metrakos PP, Chevet E. 2006. Proteomic analysis of ischemia-reperfusion injury upon human liver transplantation reveals the protective role of IQGAP1. Mol Cell Proteomics 5:1300–1313.

Farber JL, Gerson RJ. 1984. Mechanisms of cell injury with hepatotoxic chemicals. Pharmacol Rev 36:71S–75S.

Fausto N. 2000. Liver regeneration. J Hepatol 32:19–31.

Fausto N, Campbell JS, Riehle KJ. 2006. Liver regeneration. Hepatology 43:S45–S53.

Frémin C, Ezan F, Boisselier P, Bessard A, Pagès G, Pouysségur J, Baffet G. 2007. ERK2 but not ERK1 plays a key role in hepatocyte replication: An RNAi-mediated ERK2 knockdown approach in wild-type and ERK1 null hepatocytes. Hepatology 45:1035–1045.

Gerlach C, Sakkab DY, Scholzen T, Dassler R, Alison MR, Gerdes J. 1997. Ki-67 expression during rat liver regeneration after partial hepatectomy. Hepatology 26:573–578.

Hautekeete ML, Geerts A. 1997. The hepatic stellate (Ito) cell: Its role in human liver disease. Virchows Arch 430:195–207.

Higgins GM, Anderson RM. 1931. Experimental pathology of the liver. I. Restoration of the liver of the white rat following partial surgical removal. Arch Pathol 12:186–202.

Katsuno T, Umeda K, Matsui T, Hata M, Tamura A, Itoh M, Takeuchi K, Fujimori T, Nabeshima Y, Noda T, Tsukita S, Tsukita S. 2008. Deficiency of zonula occludens-1 causes embryonic lethal phenotype associated with defected yolk sac angiogenesis and apoptosis of embryonic cells. Mol Biol Cell 19:2465–2475.

Kubo A, Yuba-Kubo A, Tsukita S, Tsukita S, Amagai M. 2008. Sentan: A novel specific component of the apical structure of vertebrate motile cilia. Mol Biol Cell 19:5338–5346.

Lemaigre F, Zaret KS. 2004. Liver development update: New embryo models, cell lineage control, and morphogenesis. Curr Opin Genet Dev 14:582–590.

Li S, Wang Q, Chakladar A, Bronson RT, Bernards A. 2000. Gastric hyperplasia in mice lacking the putative Cdc42 effector IQGAP1. Mol Cell Biol 20:697–701.

Michalopoulos GK. 2007. Liver regeneration. J Cell Physiol 213:286–300.

Michalopoulos GK, DeFrances MC. 1997. Liver regeneration. Science 276:60–66.

Nojima H, Adachi M, Matsui T, Okawa K, Tsukita S, Tsukita S. 2008. IQGAP3 regulates cell proliferation through the Ras/ERK signalling cascade. Nat Cell Biol 10:971–978.

Noritake J, Watanabe T, Sato K, Wang S, Kaibuchi K. 2005. IQGA P1: A key regulator of adhesion and migration. J Cell Sci 118:2085–2092.

Parviz F, Matullo C, Garrison WD, Savatski L, Adamson JW, Ning G, Kaestner KH, Rossi JM, Zaret KS, Duncan SA. 2003. Hepatocyte nuclear factor 4alpha controls the development of a hepatic epithelium and liver morphogenesis. Nat Genet 34:292–296.

Peng Y, Murr MM. 2007. Establishment of immortalized rat Kupffer cell lines. Cytokine 37:185–191.

Schaller E, Macfarlane AJ, Rupec RA, Gordon S, McKnight AJ, Pfeffer K. 2002. Inactivation of the F4/80 glycoprotein in the mouse germ line. Mol Cell Biol 22:8035–8043.

Schmidt VA, Chiariello CS, Capilla E, Miller F, Bahou WF. 2008. Development of hepatocellular carcinoma in Iqgap2-deficient mice is IQGAP1 dependent. Mol Cell Biol 28:1489–1502.

Sugimoto N. 2001. IQGAP1, a negative regulator of cell-cell adhesion, is upregulated by gene amplification at 15q26 in gastric cancer cell lines HSC39 and 40A. J Hum Genet 46:21–25.

Talarmin H, Rescan C, Cariou S, Glaise D, Zanninelli G, Bilodeau M, Loyer P, Guguen-Guillouzo C, Baffet G. 1999. The mitogen-activated protein kinase kinase/extracellular signal-regulated kinase cascade activation is a key signalling pathway involved in the regulation of G(1) phase progression in proliferating hepatocytes. Mol Cell Biol 19:6003–6011.

Wang S, Watanabe T, Noritake J, Fukata M, Yoshimura T, Itoh N, Harada T, Nakagawa M, Matsuura Y, Arimura N, Kaibuchi K. 2007. IQGAP3, a novel effector of Rac1 and Cdc42, regulates neurite outgrowth. J Cell Sci 120:567–577.

Yamada A, Fujita N, Sato T, Okamoto R, Ooshio T, Hirota T, Morimoto K, Irie K, Takai Y. 2006. Requirement of nectin, but not cadherin, for formation of claudin-based tight junctions in annexin II-knockdown MDCK cells. Oncogene 25:5085–5102.

Zhao R, Duncan SA. 2005. Embryonic development of the liver. Hepatology 41:956–967.

Liver International ISSN 1478-3223

CLINICAL STUDIES

Oxidative stress may enhance the malignant potential of human hepatocellular carcinoma by telomerase activation

Taichiro Nishikawa, Tomoki Nakajima, Tatsuo Katagishi, Yoshihisa Okada, Masayasu Jo, Keizo Kagawa, Takeshi Okanoue, Yoshito Itoh and Toshikazu Yoshikawa

Kyoto Prefectural University of Medicine Graduate School of Medical Science, Molecular Gastroenterology and Hepatology, Kyoto, Japan

Keywords
Akt – 8-OHdG – HCC – hTERT – PTEN – telomere

Abbreviations
DAPI, 4-6-diamidino-2-phenylindole; 8-OhdG, 8-hydroxy-2′-deoxyguanosine; FITC, fluorescein isothiocyanate; HCC, human hepatocellular carcinoma; hTERT, human telomerase reverse transcriptase; OS, oxidative stress; PNA, peptide nucleic acid; PTEN, phosphatase and tensin homolog deleted on chromosome 10; ROS, reactive oxygen species; RTA, relative telomerase activity; TRAP, telomere repeat amplification protocol.

Correspondence
Taichiro Nishikawa, Kyoto Prefectural University of Medicine Graduate School of Medical Science, Molecular Gastroenterology and Hepatology, Kyoto, Japan
Tel: +81 75 251 5519
Fax: +81 75 251 0710
e-mail: liverresearch2004@yahoo.co.jp

Received 2 September 2008
Accepted 7 November 2008

DOI:10.1111/j.1478-3231.2008.01963.x

Abstract

Background/Aims: Continuous oxidative stress (OS) plays an important role in the progression of chronic liver diseases and hepatocarcinogenesis through telomere shortening in hepatocytes. However, it has not been established how the OS influences the progression of human hepatocellular carcinomas (HCCs). We examined the correlations of OS with telomere length of cancer cells, telomerase activity and other clinicopathological factors in 68 HCCs. *Methods:* The level of 8-hydroxy-2′-deoxyguanosine (8-OHdG) as a marker of OS was examined immunohistochemically and OS was scored in four grades (0–3). The telomere length of cancer cells was measured by quantitative fluorescence *in situ* hybridization. Telomerase activity was measured by (i) immunodetection of human telomerase reverse transcriptase (hTERT) and (ii) telomere repeat amplification protocol (TRAP) assay. Telomerase related proteins, phosphatase and tensin homolog deleted on chromosome 10 (PTEN) and Akt, and other clinicopathological factors were also evaluated. *Results:* As the OS grade increased, the average telomere length became significantly shorter in HCCs, especially in the hTERT-negative group. In the state of high-grade OS, hTERT-positive HCC cells showed more proliferative and less apoptotic features compared with hTERT-negative HCC cells. Telomerase activity, as measured by the TRAP assay, was strongly correlated with OS grade in HCCs. Furthermore, a high OS grade was correlated with the downexpression of PTEN and the activation of Akt. *Conclusions:* Oxidative stress enhanced the malignant potential of HCCs through the activation of telomerase, which raises the possibility of using OS as a marker for assessing the clinical state of HCCs.

Continuous oxidative stress (OS), which results from the generation of reactive oxygen species (ROS) by environmental factors or cellular mitochondrial dysfunction, has recently been associated with the progression of chronic liver diseases and hepatocarcinogenesis (1–3). Repeated necrosis and regeneration of hepatocytes induced by OS appear to accelerate the senescence of hepatocytes, giving them the appearance of cancer cells. These processes may be due to the shortening of the telomeres of hepatocytes.

Telomeres, hexameric DNA repeats $(TTAGGG)_n$ at the ends of chromosomes (4), increase chromosomal stability by preventing chromosomal rearrangements and end-to-end fusions. In normal somatic cells, telomere shortening occurs during each cell division (5) and eventually leads to cell cycle arrest and apoptosis (6). In cancer cells, the length of telomeres is maintained by the expression of telomerase, which endows cancer cells with immortality and an ability to proliferate without any limit.

OS accelerates the shortening of the telomeres of human cells by inducing oxidative single-stranded damage in telomeric DNA (7, 8). Fibrosis and cirrhosis in liver have been attributed to OS-induced telomere shortening (9, 10). In hepatocytes, telomere shortening can be carcinogenic because it can lead to genetic changes such as telomerase activation (11). Whereas OS has such effects on normal liver cells, it is unclear whether it also has a role in the progression of hepatic cancer cells, especially with respect to telomeres and telomerase.

In this study, we investigated the effects of OS in human hepatocellular carcinomas (HCCs). Our findings indicate that OS promotes the development of HCCs and increases

their resistance to treatment and is associated with shortened telomeres and increased telomerase activity.

Materials and methods

Tissue preparation and patients

All HCC specimens were obtained from 63 patients who underwent partial hepatectomy and five patients who underwent needle biopsy in 1992–2005 in Kyoto Prefectural University of Medicine. None of the specimens had undergone any treatments such as percutaneous ethanol injection therapy or transcatheter arterial embolization before the collections. The clinicopathological parameters of these patients and the clinicopathological status of their HCC samples are shown in Table 1. Fourteen patients were positive for serum hepatitis B surface antigen, 45 were positive for anti-hepatitis C antibody, one was positive for both and eight were negative for both. Of the 68 patients, two had normal livers, 29 had chronic hepatitis and 37 had liver cirrhosis. Specimens were fixed in 4% buffered paraformaldehyde for 12–24 h, embedded in paraffin and cut into 5-μm-thick sections for use as described below. All 68 HCC paraffin blocks included non-cancerous tissues, which served as controls. Additionally, parts of 30 specimens were stored at − 80 °C for later use in the telomere repeat amplification protocol (TRAP) assay (described below). Sixty-eight HCC specimens were stained with haematoxylin and eosin and classified according to their differentiation status according to the criteria of the Liver Cancer Study Group of Japan. Of these specimens, 29 were classified as well differentiated, 28 were classified as moderately differentiated and 11 were classified as poorly differentiated. The degree of necroinflammatory activity and fibrosis of non-cancerous tissues were classified according to the international classification (12) by haematoxylin and eosin and Masson trichrome staining. Informed consent to our using HCC specimens for this study was obtained from all patients according to the guidelines approved by our hospital ethical committee.

Table 1. Age and sex of 68 human hepatocellular carcinoma patients and the clinicopathological status of their human hepatocellular carcinoma samples

Sex	
Male	43
Female	25
Age (years) (mean ± SD)	
Range	25–77
Mean ± SD	62.6 ± 8.15
Aetiology	
HBV	14
HCV	45
HBV+HCV	1
Non-HBV, non-HCV	8
Non-cancerous tissue	
Normal liver	2
Chronic hepatitis	29
Liver cirrhosis	37
Tumour size (mm)	12–160
Tumour stage	
I	10
II	46
III	9
IV	3
Tumour differentiation	
Well differentiated	29
Moderately differentiated	28
Poorly differentiated	11

HBV, hepatitis B virus; HCV, hepatitis C virus; SD, standard deviation.

Immunohistochemical analysis

Sections were deparaffinized, immersed in 0.3% H_2O_2–methanol for 20 min, autoclaved at 120 °C for 20 min in a Target Retrieval Solution (DakoCytomation, Kyoto, Japan), incubated in blocking buffer (Tris buffered saline containing 2% fetal bovine serum) to block non-specific reactions and incubated with one of the four primary antibodies diluted 1:100 in the blocking buffer at 4 °C overnight. The antibodies were mouse anti-Ki-67 monoclonal antibody (DakoCytomation), rabbit anti-phosphatase and tensin homolog deleted on chromosome 10 (PTEN) monoclonal antibody (Cell Signaling Technology Inc., Beverly, MA, USA) and rabbit anti-phospho-AKT (Ser473) monoclonal antibody (Cell Signaling Technology Inc.). The remaining procedure was based on the standard streptavidin–biotin–peroxidase complex method (13). Positive reactions were visualized using diaminobenzidine (DAB; Wako, Osaka, Japan) as a substrate. The sections were counterstained with haematoxylin. Each immunohistochemical analysis included a slide without the primary antibody as a negative control. The Ki-67 index, an indicator of tumoral proliferative activity, was defined as the number of Ki-67 antibody-positive cells per 1000 scored cancer cells.

8-Hydroxy-2′-deoxyguanosine immunohistochemistry

Following the method of Kato *et al.* (13), 1000–2000 cancer or normal hepatic cells from HCC or non-cancerous tissues were stained with antibody against 8-hydroxy-2′-deoxyguanosine (8-OhdG), a marker of oxidative DNA damage. Immunoreactive cells were detected as described above and were counted by two hepatologists (T. N. and T. N.). The degree of OS was classified according to the percentage of 8-OhdG-positive cells: Grade 0, < 10%; Grade 1, 10–50%; Grade 2, 50–90%; Grade 3, > 90%.

Human telomerase reverse transcriptase immunohistochemistry

Human telomerase reverse transcriptase (hTERT), a telomerase catalytic subunit, is an indicator of telomerase activity in cancer cells (14). hTERT was immunohistochemically detected with mouse anti-hTERT monoclonal antibody (Novocastra, Newcastle Upon Tyne, UK) as